Self-Assembly, Spectroscopic, and Electrochemical Properties of [*n*]Rotaxanes[1]

Peter R. Ashton,[†] Roberto Ballardini,[⊥] Vincenzo Balzani,[§] Martin Bělohradský,[†] Maria Teresa Gandolfi,[§] Douglas Philp,[†] Luca Prodi,[§] Francisco M. Raymo,[†] Mark V. Reddington,[†] Neil Spencer,[†] J. Fraser Stoddart,*,[†] Margherita Venturi,[§] and David J. Williams[‡]

Contribution from The School of Chemistry, The University of Birmingham, Edgbaston, Birmingham B15 2TT, UK, The Chemical Crystallography Laboratory, Department of Chemistry, Imperial College, South Kensington, London SW7 2AY, UK, Istituto FRAE-CNR, via Gobetti 101, I-40129 Bologna, Italy, and Dipartimento di Chimica "G. Ciamician" dell'Università, via Selmi 2, I-40126 Bologna, Italy

Received December 29, 1995[⊗]

Abstract: Synthetic approaches to self-assembling [*n*]rotaxanes incorporating π-electron deficient bipyridinium-based dumbbell-shaped components and π-electron rich hydroquinone-based macrocycles have been developed. In particular, the so-called slippage methodology relies upon the size complementarity of preformed macrocyclic and dumbbell-shaped components. The spontaneous self-assembly of these complementary components into a rotaxane in solution can be achieved under the influence of an appropriate amount of thermal energy. The absorption spectra, luminescence properties, and electrochemical behavior of the rotaxanes and their dumbbell-shaped components have been investigated and discussed on the basis of the behavior of their chromophoric and electroactive units. Charge-transfer and energy-transfer processes between specific chromophoric subunits and unusual correlations between the redox patterns of the various compounds have been evidenced and interpreted.

Introduction

Previously, we have shown[2] that the bipyridinium-based herbicide paraquat[3] forms a 1:1 pseudorotaxane-like complex with bis-*p*-phenylene-34-crown-10 (BPP34C10), both in solution and in the solid state. Noncovalent bonding interactions—namely, π−π stacking[4] between the complementary aromatic units in addition to hydrogen bonding[5] between the polyether oxygen atoms and the acidic (Me and α-bipy) protons of paraquat—are responsible for the self-assembly[6] of this [2]pseudorotaxane. This result suggested to us the possibility of generating rotaxanes based on linear components incorporating bipyridinium units and the macrocyclic component BPP34C10. We have been able
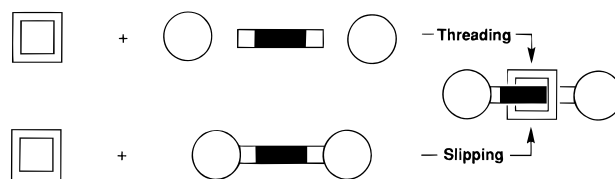

Figure 1. The threading and slipping approaches to self-assembling [2]rotaxanes.

to devise two different synthetic approaches to such rotaxanes (Figure 1): they involve threading and slipping. In the case of threading,[7] the complexation between a preformed macrocycle and a rod-like component is followed by the covalent bonding of two stoppers to prevent the unthreading of the macrocycle from the dumbbell-shaped component. In the case of slipping,[8] the macrocycle and the dumbbell-shaped components are preformed separately and then cajoled into associating one with the other (Figure 2) under the influence of an appropriate amount of thermal energy.

Apart from synthetic aspects, rotaxanes are very interesting molecular species from the viewpoint of spectroscopic and electrochemical investigations. In the rotaxanes and in their "free" dumbbell-shaped and macrocyclic components, one can

* Corresponding author: Professor J. Fraser Stoddart, School of Chemistry, University of Birmingham, Edgbaston, Birmingham B15 2TT (UK). Fax: +44-121-414-3531.
 [†] University of Birmingham.
 [‡] Imperial College.
 [⊥] FRAE-CNR.
 [§] University of Bologna.
 [⊗] Abstract published in *Advance ACS Abstracts,* May 1, 1996.

(1) Molecular Meccano, Part 9. For Part 8, see: Asakawa, M.; Ashton, P. R.; Menzer, S.; Raymo, F. M.; Stoddart, J. F.; White, A. J. P.; Williams, D. J. *Chem. Eur. J.* In press.

(2) (a) Allwood, B. L.; Spencer, N.; Shahriari-Zavareh, H.; Stoddart, J. F.; Williams, D. J. *J. Chem. Soc., Chem. Commun.* **1987**, 1064−1066. (b) Ashton, P. R.; Slawin, A. M. Z.; Spencer, N.; Stoddart, J. F.; Williams, D. J. *J. Chem. Soc., Chem. Commun.* **1987**, 1066−1069. (c) Stoddart, J. F. *Pure Appl. Chem.* **1988**, *60*, 467−472. (d) Ashton, P. R.; Philp, D.; Reddington, M. V.; Slawin, A. M. Z.; Spencer, N.; Stoddart, J. F.; Williams, D. J. *J. Chem. Soc., Chem. Commun.* **1991**, 1680−1683.

(3) Summers, L. A., *The Bipyridinium Herbicides*, Academic Press: London, 1980.

(4) (a) Hunter, C. A.; Sanders, J. K. M. *J. Am. Chem. Soc.* **1990**, *112*, 5525−5534. (b) Hunter, C. A. *Angew. Chem., Int. Ed. Engl.* **1993**, *32*, 1584−1586; (c) Hunter, C. A. *J. Mol. Biol.* **1993**, *230*, 1025−1054. (d) Hunter, C. A. *Chem. Soc. Rev.* **1994**, *23*, 101−109.

(5) (a) Etter, M. C. *Acc. Chem. Res.* **1990**, *23*, 120−126. (b) Aakeröy, C. B.; Seddon, K. R. *Chem. Soc. Rev.* **1993**, *22*, 397−407. (c) Desiraju, G. R. *Angew. Chem., Int. Ed. Engl.* **1995**, *34*, 2311−2327.

(6) (a) Lindsey, J. S. *New J. Chem.* **1991**, *15*, 153−180. (b) Whitesides, G. M.; Mathias, J. P.; Seto, C. T. *Science* **1991**, *254*, 1312−1319. (c) Whitesides, G. M.; Simanek, E. E.; Mathias, J. P.; Seto, C. T.; Chin, D. N.; Mammen, M.; Gordon, D. *Acc. Chem. Res.* **1995**, *28*, 37−44. (d) Lawrence, D. S.; Jiang, T.; Levett, R. *Chem. Rev.* **1995**, *95*, 2229−2260. (e) Raymo, F. M.; Stoddart, J. F. *Curr. Op. Coll. Interf. Sci.* **1996**, *1*, 116−126. (f) Philp, D.; Stoddart J. F. *Angew. Chem., Int. Ed. Engl.* In press.

(7) Ashton, P. R.; Philp, D.; Spencer, N.; Stoddart, J. F. *J. Chem. Soc., Chem. Commun.* **1992**, 1124−1128.

(8) (a) Ashton, P. R.; Bělohradský, M.; Philp, D.; Stoddart, J. F. *J. Chem. Soc., Chem. Commun.* **1993**, 1269−1274. (b) Ashton, P. R.; Bělohradský, M.; Philp, D.; Spencer, N.; Stoddart, J. F. *J. Chem. Soc., Chem. Commun.* **1993**, 1274−1277. (c) Amabilino, D. B.; Ashton, P. R.; Bělohradský, M.; Raymo, F. M.; Stoddart, J. F. *J. Chem. Soc., Chem. Commun.* **1995**, 747−750. (d) Amabilino, D. B.; Ashton, P. R.; Bělohradský, M.; Raymo, F. M.; Stoddart, J. F. *J. Chem. Soc., Chem. Commun.* **1995**, 751−753.

Scheme 1

Scheme 2
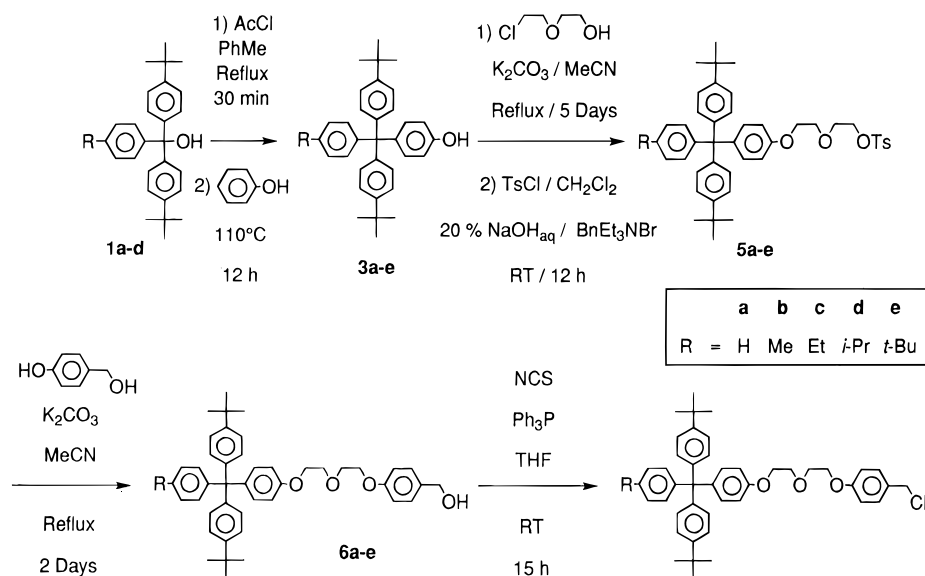
single out several chromophoric and electroactive units and study their interactions which often lead to charge-transfer and energy-transfer processes and to very unusual redox patterns. Because of these interactions, rotaxanes and related systems are interesting for the design of chemically-,[9] photochemically-,[10] and electrochemically-active[9a,11] molecular devices. Here, we report the self-assembly of a range of [2]-, [3]-, and [4]-rotaxanes, incorporating π-electron deficient bipyridinium-based components encircled by one or more hydroquinone-based components as well as the investigation of their spectroscopic and electrochemical properties.
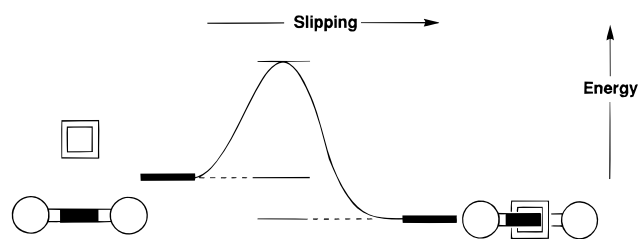

Figure 2. The thermodynamically-driven formation of a [2]rotaxane by slipping.

Results and Discussion

Synthesis.[12] The stable and highly crystalline alcohols **6a–e** were prepared according to the synthetic route shown in Scheme 1. They served as stock compounds for the preparation of the corresponding benzylic chlorides by reaction with *N*-chlorosuccinimide and Ph$_3$P in dry THF at room temperature during 15 h. The resulting chlorides were purified by fast filtration through a silica-gel bed and used immediately in the next step without further purification.

(9) (a) Bissell, R. A.; Córdova, E.; Kaifer, A. E.; Stoddart, J. F. *Nature* **1994**, *369*, 133–137. (b) Ballardini, R.; Balzani, V.; Credi, A.; Gandolfi, M. T.; Langford, S. J.; Menzer, S.; Prodi, L.; Stoddart, J. F.; Venturi, M.; Williams, D. J. *Angew. Chem., Int. Ed. Engl.* **1996**, *35*, 1056–1059.

(10) (a) Ballardini, R.; Balzani, V.; Gandolfi, M. T.; Prodi, L.; Venturi, M.; Philp, D.; Ricketts, H. G.; Stoddart J. F. *Angew. Chem., Int. Ed. Engl.* **1993**, *32*, 1301–1303. (b) Benniston, A. C.; Harriman, A.; Lynch, V. M. *J. Am. Chem. Soc.* **1995**, *117*, 5275–5291.

(11) (a) Livoreil, A.; Dietrich-Buchecker, C. O.; Sauvage, J. P. *J. Am. Chem. Soc.*, **1994**, *116*, 9399–9400. (b) Ashton, P. R.; Ballardini, R.; Balzani, V.; Credi, A.; Gandolfi, M. T.; Marquis, D. J. F..; Menzer, S.; Pérez-Garcia, L.; Prodi, L.; Stoddart, J. F.; Venturi, M.; White, A. J. P.; Williams, D. J. *J. Am. Chem. Soc.* **1995**, *117*, 11171–11197.

The dumbbell-shaped compounds **7a–e**,[7,8a] **9a**,[8b] and **12c** incorporating one, two, and three bipyridinium recognition sites, respectively, were synthesized as shown in Schemes 2–4, respectively.
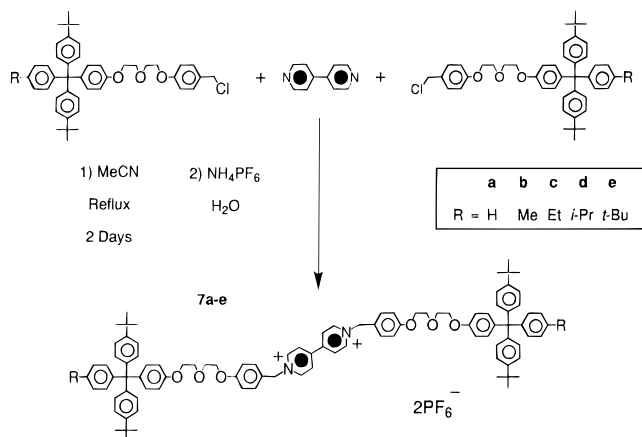
The threading approach to rotaxanes is based on the mutual recognition between the π-electron deficient 4,4′-bipyridinium recognition site(s) incorporated within the linear precursor and

(12) Acronyms composed of letters and numbers are employed throughout the text, and the illustrations for the compounds bis-*p*-phenylene-34-crown-10 (BPP34C10), bis[4-(4-pyridyl)pyridinium]-*p*-xylylene bis(hexafluorophosphate) ([BPYPYXY][PF$_6$]$_2$), *N,N′*-bis(α-bromo-*p*-xylene)-4,4′-bipyridinium bis(hexafluorophosphate) ([BBXYBIPY][PF$_6$]$_2$), *N,N′*-bis[α-[4-(4-pyridyl)pyridinium]-*p*-xylylene]-4,4′-bipyridinium tetrakis(hexafluorophosphate) ([BPYPYXYBIPY][PF$_6$]$_4$), *N,N′*-bis(methyl)-4,4′-bipyridinium bis(hexafluorophosphate) ([PQT][PF$_6$]$_2$), *N,N′*-bis(hydro)-4,4′-bipyridinium bis(hexafluorophosphate) ([BHBIPY][PF$_6$]$_2$), *N,N′*-bis(2-hydroxyethyl)-4,4′-bipyridinium bis(hexafluorophosphate) ([BHEBIPY][PF$_6$]$_2$), *N,N′*-bis-[2-(2-hydroxyethoxy)ethyl]-4,4′-bipyridinium bis(hexafluorophosphate) ([BHEEBIPY][PF$_6$]$_2$). Numbers are also employed throughout the text and in the illustrations for all the remaining compounds. In the cartoon version of the rotaxanes, each dark rectangle incorporated within the dumbbell-shaped component represents a bipyridinium recognition site carrying two positive charges. The dicationic nature of this site is not indicated by plus charges: it is implied by the dark (shaded) rectangle. The circles at both ends of the rod-like derivative correspond to the substituted tetraarylmethane stopper units. The two *tert*-butyl groups attached to each stopper are represented by the usual shorthand notation, while the third substituent is indicated by more traditional alphabetical abbreviations. Each of the BPP34C10 macrocycles encircling the dumbbell-shaped component is represented by an open (unshaded) square.
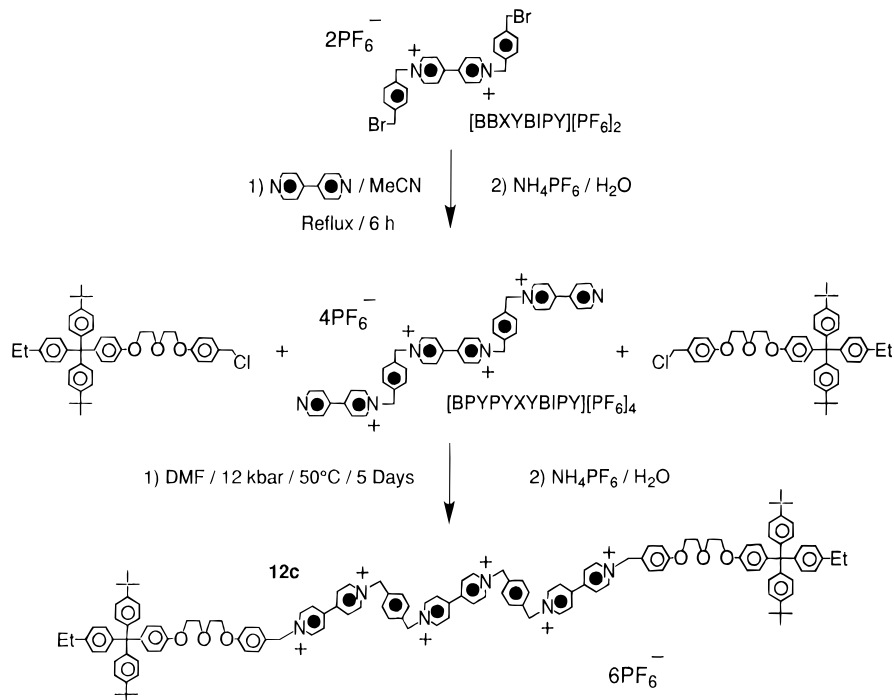
Scheme 3
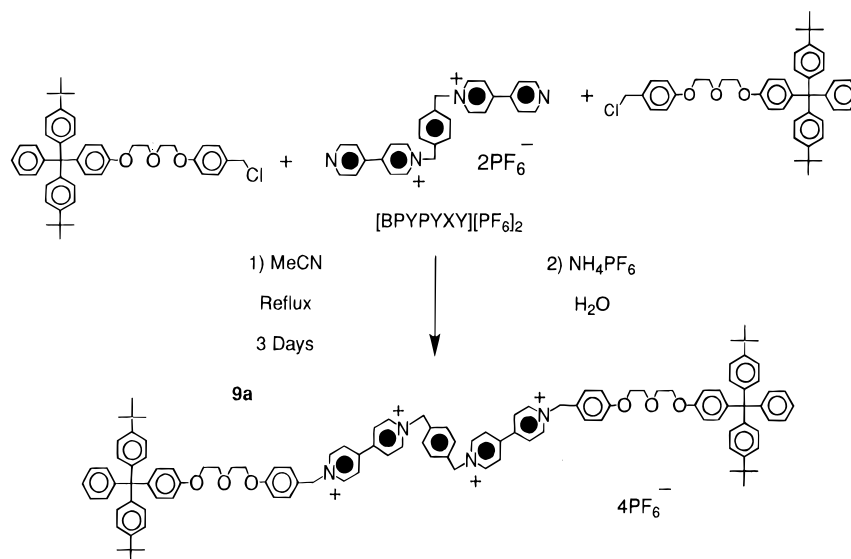
the π-electron rich macrocyclic polyether BPP34C10. A pronounced effect of ultrahigh pressure on the self-assembly processes was observed when the threading methodology was employed. When 4,4′-bipyridine was reacted (Scheme 5) with an excess of the tris(4-*tert*-butylphenyl)methyl-based chloride in the presence of BPP34C10 in MeCN at ambient temperature and pressure, only the free dumbbell-shaped compound **7e** was isolated from the reaction mixture: no rotaxane was detected. However, reaction in DMF at 30 °C for 2 days under ultrahigh pressure gave the [2]rotaxane **8e**, after counterion exchange, in a yield of 26%. Furthermore, treating a DMF solution of the preformed dumbbell-shaped compound **7e** and BPP34C10 under ultrahigh pressure yields back again the free dumbbell-shaped and macrocyclic components. Thus, the passage of the BPP34C10 macrocycle over the tris(4-*tert*-butylphenyl)methyl-based stoppers is not possible even under these conditions. Presumably, the formation of a complex with pseudorotaxane-like geometry between BPP34C10 and the π-electron deficient

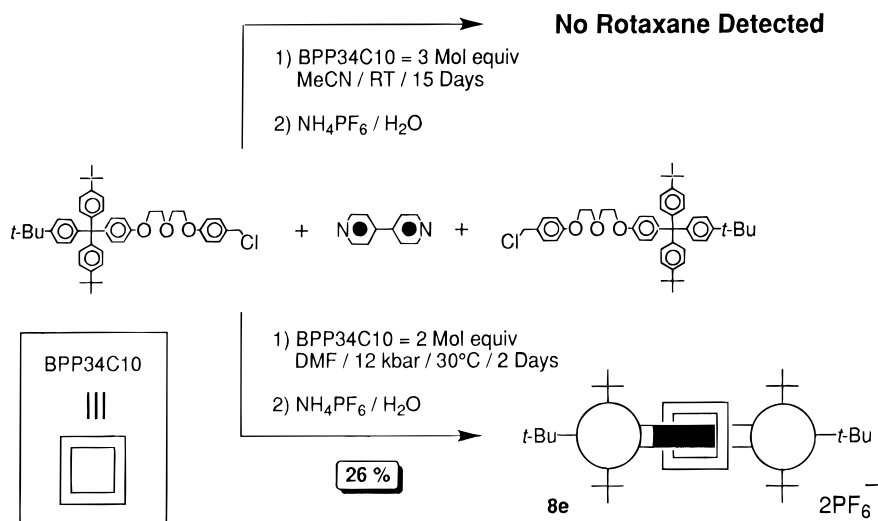rod-like derivative is highly favored under ultrahigh pressure conditions.

A similar effect of ultrahigh pressure was observed during the self-assembly of the rotaxanes **10e** and **11e**. The alkylation of [BBIPYXY][PF$_6$]$_2$ with an excess of the tris(4-*tert*-butyl-phenyl)methyl-based chloride in the presence of 1.5 molar equiv of BPP34C10 in DMF under ultrahigh pressure conditions afforded (Scheme 6) the [2]rotaxane **10e** and [3]rotaxane **11e** in yields of 18 and 3%, respectively, after counterion exchange. By employing 4 molar equiv of the macrocycle BPP34C10 under otherwise identical conditions, the yields of **10e** and **11e** became 5 and 33%, respectively. Thus, the proportions of the [2]rotaxane **10e** and the [3]rotaxane **11e** are influenced dramatically by the ratio of BPP34C10 to the linear precursor [BBIPYXY][PF$_6$]$_2$.

The self-assembly of rotaxanes incorporating three bipyridinium recognition sites along the dumbbell-shaped component was also achieved by employing the threading methodology.
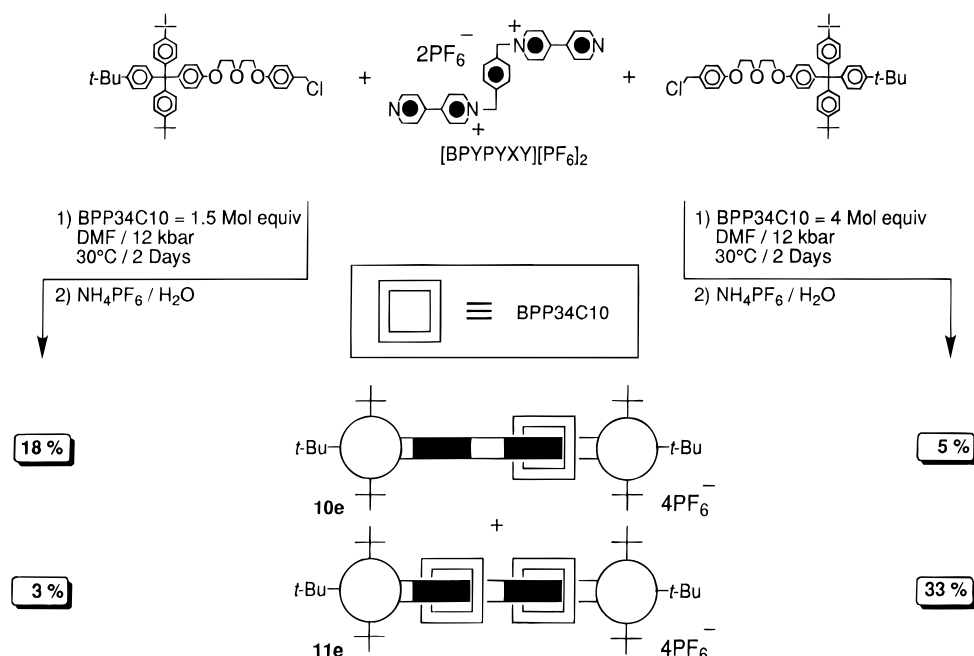
Scheme 4

Scheme 5

No Rotaxane Detected

1) BPP34C10 = 3 Mol equiv
   MeCN / RT / 15 Days

2) NH$_4$PF$_6$ / H$_2$O

t-Bu——⬡——⬡—O⬡O O O⬡—Cl   +   N⬡——⬡N   +   Cl—⬡O O O⬡O——⬡——*t*-Bu

BPP34C10

‖‖‖
□

1) BPP34C10 = 2 Mol equiv
   DMF / 12 kbar / 30°C / 2 Days

2) NH$_4$PF$_6$ / H$_2$O

26 %

t-Bu——◯——█——◯——*t*-Bu

8e   2PF$_6^-$

Reaction of [BPYPYXYBIPY][PF$_6$]$_4$ with an excess of the tris-(4-*tert*-butylphenyl)methyl-based chloride in the presence of only 2.2 molar equiv of BPP34C10 in DMF under ultrahigh pressure gave (Scheme 7) the [4]rotaxane **15e** and the [3]-rotaxane **14e** in yields of 3 and 1%, respectively, while only traces of the [2]rotaxane **13e** were obtained. Interestingly, the [4]rotaxane **15e** was obtained in higher yields with respect to the [3]rotaxane **14e**, despite the fact that only 2.2 molar equiv of macrocycle were employed. The solubility of the pseudoro-taxane intermediates is highly affected by the number of macrocyclic units threaded on to the linear derivative and by nature of the counterions. Presumably, the more soluble [4]-pseudorotaxane predominates in solution in the presence of chloride counterions, leading to the fully occupied [4]rotaxane **15e** as the major product amongst the rotaxanes.
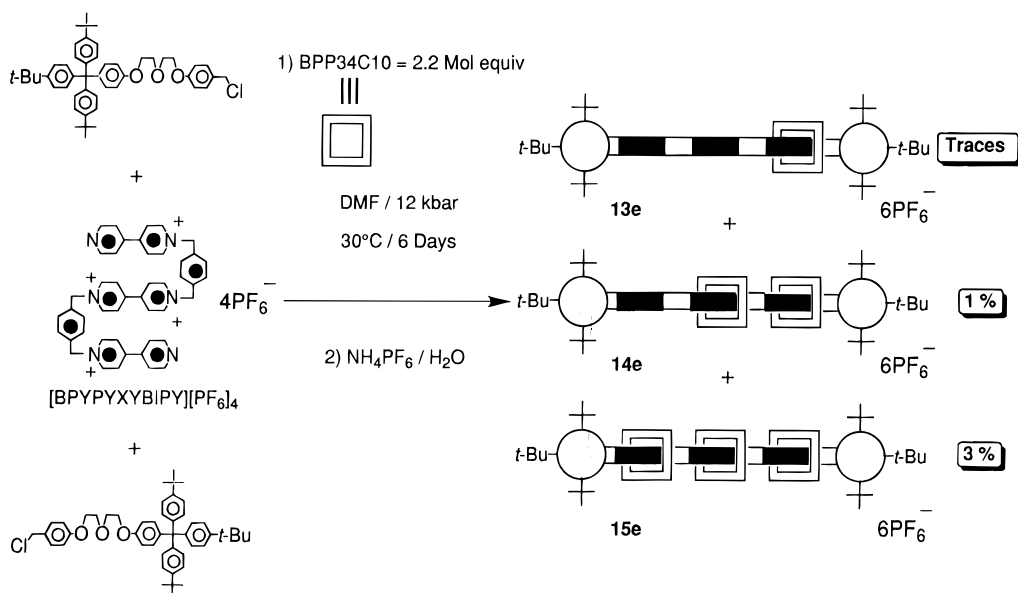
The tris-(4-*tert*-butylphenyl)methyl-based stoppers of the rotaxanes, prepared by threading, were designed to be large enough to prevent the passage of BPP34C10 over them. We reasoned that, by sensible adjustment of the size of the stoppers, we could arrive at a situation where the size complementarity between the BPP34C10 ring and the tetraarylmethane stoppers

was such that the slipping of macrocycle over them would eventually become possible. As a result of noncovalent bonding interactions, the bipyridinium recognition site, situated within the dumbbell-shaped component, provides a "thermodynamic trap" by raising the activation energy (Figure 2) for the extrusion—*i.e.*, decomplexation—process relative to that for the assembly process—*i.e.*, complexation. In order to investigate the slipping process, we synthesized the dumbbell-shaped compounds **7a**−**d**, incorporating one bipyridinium unit in which the size of the stoppers was varied systematically. By heating these dumbbell-shaped compounds **7a**−**d** with an excess of BPP34C10 macrocycle in MeCN at 55 °C for 10 days, the [2]-rotaxanes **8a**−**c** were self-assembled[8a] (Scheme 8) in good yields. By contrast, when the dumbbell-shaped compound **7d**, containing the 4-isopropylphenylbis(4-*tert*-butylphenyl)methyl-based stoppers, was employed under otherwise identical conditions, no rotaxane was detected.[8a] Thus, the barrier to slipping of the BPP34C10 macrocycle over the stoppers of the dumbbell-shaped component is reached on going from the "Et-substituted" to the "*i*-Pr-substituted" stoppers.

Scheme 6

t-Bu——⬡——⬡—O⬡O O O⬡—Cl   +   2PF$_6^-$ $\overset{+}{N}$⬡——⬡N   +   Cl—⬡O O O⬡O——⬡——*t*-Bu

N⬡——⬡$\overset{+}{N}$

[BPYPYXY][PF$_6$]$_2$

1) BPP34C10 = 1.5 Mol equiv
   DMF / 12 kbar
   30°C / 2 Days

2) NH$_4$PF$_6$ / H$_2$O

□
□   ≡   BPP34C10

1) BPP34C10 = 4 Mol equiv
   DMF / 12 kbar
   30°C / 2 Days

2) NH$_4$PF$_6$ / H$_2$O

18 %   5 %

t-Bu——◯——█—█——◯——*t*-Bu

10e   4PF$_6^-$

+

3 %   33 %

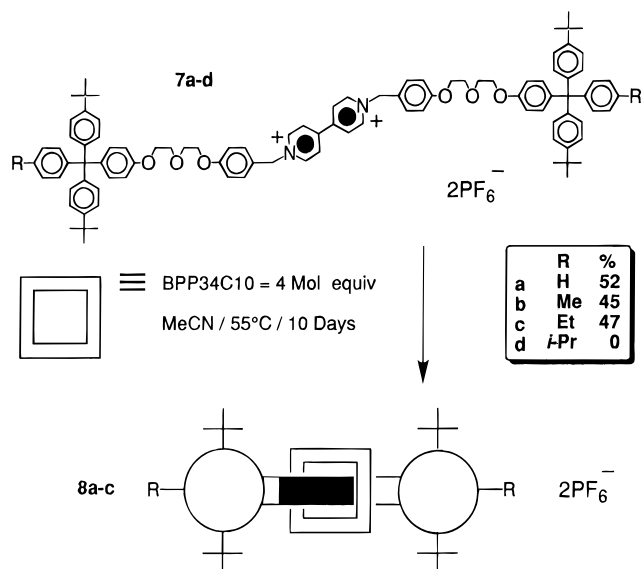*t*-Bu——◯——█——█——◯——*t*-Bu

11e   4PF$_6^-$

Scheme 7

Scheme 8

Although the size complementarity concept has been applied previously[13] in the statistical synthesis of [2]rotaxanes, the addition of noncovalent bonding interactions increases dramatically the yield and contributes to the inherent stability and information content of the resulting molecular structures. These factors, and the synthetic simplicity of the slipping approach, recommend this method as an alternative synthetic procedure for construction of larger oligorotaxanes and polyrotaxanes. Thus, we also employed the slipping methodology to self-assemble rotaxanes incorporating two and three bipyridinium recognition sites within the dumbbell-shaped component. By heating the dumbbell-shaped compound **9a**, incorporating two bipyridinium units, with 4 molar equiv of BPP34C10 in MeCN at 55 °C for 10 days, the [2]rotaxane **10a** and the [3]rotaxane **11a** were self-assembled[8b] (Scheme 9) in yields of 31 and 8%, respectively. When 10 molar equiv of the macrocyclic polyether were employed under otherwise identical conditions, the [2]-rotaxane **10a** and the [3]rotaxane **11a** were self-assembled[8b] in yields of 20 and 55%, respectively. Thus, as expected, the proportions of the [2]rotaxane **10a** and the [3]rotaxane **11a** are

(13) Harrison, I. T. *J. Chem. Soc., Chem. Commun.* **1972**, 231−232.

dramatically influenced by the molar ratio of the BPP34C10 macrocycle to the dumbbell-shaped compound **9a**.
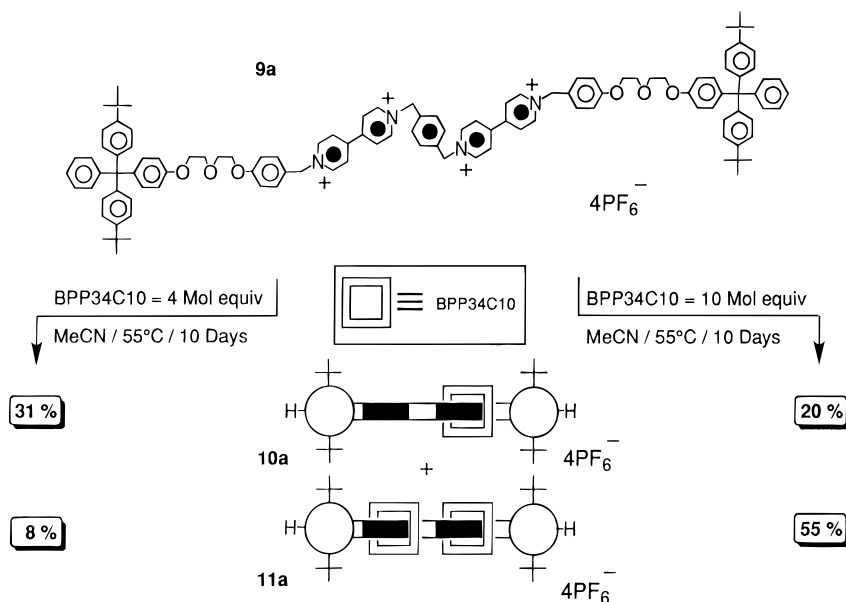
Rotaxanes incorporating three bipyridinium recognition sites within the dumbbell-shaped component have also been self-assembled using the slipping approach. Heating the dumbbell-shaped compound **12c**, incorporating three bipyridinium units, with 2 molar equiv of BPP34C10 in MeCN at 55 °C for 10 days afforded (Scheme 10) the [2]rotaxane **13c**, the [3]rotaxane **14c**, and the [4]rotaxane **15c** in yields of 19, 10, and 4%, respectively. When 20 molar equiv of BPP34C10 were employed under otherwise identical conditions, the [2]rotaxane **13c**, the [3]rotaxane **14c**, and the [4]rotaxane **15c** were self-assembled in yields of 2, 12, and 19%, respectively. Once more, we note that the proportions of the rotaxane products can be controlled by changing the molar ratio of BPP34C10 to the dumbbell-shaped component.

X-ray Crystal Structures. The X-ray crystallographic analysis of the 1:1 complexes [BPP34C10-BHBIPY][PF$_6$]$_2$, [BPP34C10-BHEBIPY][PF$_6$]$_2$, and [BPP34C10-BHEEBIPY]-[PF$_6$]$_2$ revealed[2d] (Figures 3−5, respectively) geometries very similar to that observed[2a] in the case of [BPP34C10-PQT][PF$_6$]$_2$. In all three structures, the bipyridinium units are inserted[14] centrosymmetrically within the cavity of the macrocyclic polyether BPP34C10. In [BPP34C10-BHBIPY]$^{2+}$, the tilt angle between the [N···N] vectors of the bipyridinium unit and the [O···O] vectors of the hydroquinone rings is only 4° as a consequence of [N-H···O] hydrogen bonding[15] (Figure 3). By contrast, the dicationic guests [BHEBIPY]$^{2+}$, [BHEEBIPY]$^{2+}$, and [PQT]$^{2+}$ within the corresponding 1:1 complexes are inserted through the cavity of BPP34C10 with tilt angles of 26, 27, and 29°, respectively. In the case where [BHEBIPY]$^{2+}$ and [BHEEBIPY]$^{2+}$ are guests, there are [C−H···O] hydrogen bonding interactions[16] between one of the CH$_2$−N hydrogen atoms of the guest and the "central" oxygen of the polyether
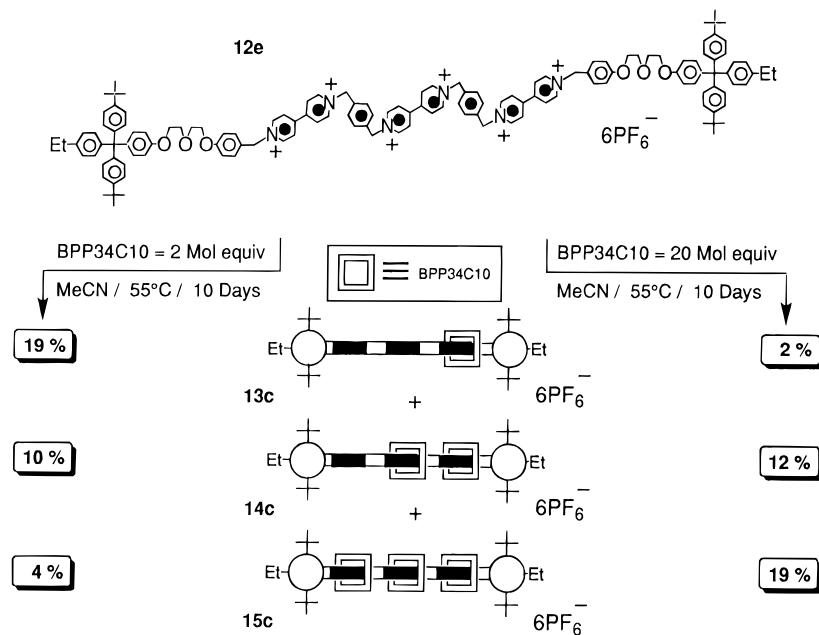
(14) The separations between the centroid of one of the centrosymmetrically-related hydroquinone rings and the centroid of the bond linking the pyridinium rings within the bipyridinium units are 3.57, 3.52, and 3.43 Å, for [BPP34C10-BHBIPY][PF$_6$]$_2$, [BPP34C10-BHEBIPY][PF$_6$]$_2$, and [BPP34C10-BHEEBIPY][PF$_6$]$_2$, respectively, *cf.* 3.72 Å in the case of [BPP34C10-PQT][PF$_6$]$_2$.

(15) [BHBIPY]$^{2+}$ is encapsulated by the macrocylic host as a result of [N-H···O] hydrogen bonding interactions between the NH hydrogen atoms on the bipyridinium unit and the "central" oxygen atom within the polyether chains of the macrocycle ([N−H...O] and [H···O] distances, 2.83 and 1.94 Å, respectively, [N−H···O] angle 174°).

Scheme 9

9a

4PF$_6^-$

BPP34C10 = 4 Mol equiv
MeCN / 55°C / 10 Days

BPP34C10 = 10 Mol equiv
MeCN / 55°C / 10 Days

□ ≡ BPP34C10

31 %

10a   +   4PF$_6^-$

20 %

8 %

11a   4PF$_6^-$

55 %

Scheme 10

12e

6PF$_6^-$

BPP34C10 = 2 Mol equiv
MeCN / 55°C / 10 Days

BPP34C10 = 20 Mol equiv
MeCN / 55°C / 10 Days

□ ≡ BPP34C10

19 %

13c   +   6PF$_6^-$

2 %

10 %

14c   +   6PF$_6^-$

12 %

4 %

15c   6PF$_6^-$

19 %

chains. Differences are observed in the conformations associated with the O−CH$_2$ bonds protruding from the hydroquinone rings. Whereas an *anti*-conformation is observed for [BPP34C10-BHBIPY][PF$_6$]$_2$ and [BPP34C10-PQT][PF$_6$]$_2$, *syn*-conformations are exhibited by [BPP34C10-BHEBIPY][PF$_6$]$_2$ and [BPP34C10-BHEEBIPY][PF$_6$]$_2$.

In the case of [BPP34C10-BHBIPY][PF$_6$]$_2$, the complexes are stacked (Figure 6) along the crystallographic *b* direction creating continuous channels within which the dications are located. The overall free pathway is restricted by the partial intrusion of the hexafluorophosphate anions. Adjacent channels are arranged with the hydroquinone rings in one stack oriented parallel to those in the next, but off-set to a degree so as to exclude any π−π interactions. The closest interstack contact is between one of the OCH$_2$ hydrogen atoms in one stack and

a hydroquinone ring of an adjacent stack, the [H···π] distance is just over 3 Å and thus could only constitute a very weak [C−H···π] interaction.

In the case of [BPP34C10-BHEBIPY][PF$_6$]$_2$, the included Me$_2$CO molecule, which is positioned on a crystallographic C_2 axis serves to link (Figure 7) adjacent threads, forming a continuous hydrogen bonded chain and hence a pseudopolyrotaxane-like superstructure. The associated [O···O], [H···O] distances and [O-H···O] angles are 2.86, 1.88 Å, and 167°, respectively. Adjacent pseudopolyrotaxanes are oriented with the hydroquinone rings in one array aligned parallel, but slightly off-set with respect to those of the next. This shearing precludes any interstack π−π interactions, but one of the OCH$_2$ hydrogen atoms within one stack is directed into the face of the hydroquinone ring of an adjacent stack and *vice versa*. The geometry of these pairs of [C−H···π] interactions must be responsible for a degree of interstack stabilization (the [H···π] distance is 2.80 Å and the [C−H···π] angle is 146°).

(16) The [C−H···O], [C···O] distances and the [C−H···O] angles are 2.51, 2.86 Å, and 167°, 2.24, 3.13 Å, and 155° for [BPP34C10-BHEBIPY]-[PF$_6$]$_2$ and [BPP34C10-BHEEBIPY][PF$_6$]$_2$, respectively, *cf.* 2.51, 3.33 Å, and 180° in the case of [BPP34C10-PQT][PF$_6$]$_2$.

Figure 3. Ball-and-stick representation of the supramolecular geometry adopted by the 1:1 complex [BPP34C10-BHBIPY][PF$_6$]$_2$ in the crystal.

Figure 4. Ball-and-stick representation of the supramolecular geometry adopted by the 1:1 complex [BPP34C10-BHEBIPY][PF$_6$]$_2$ in the crystal.
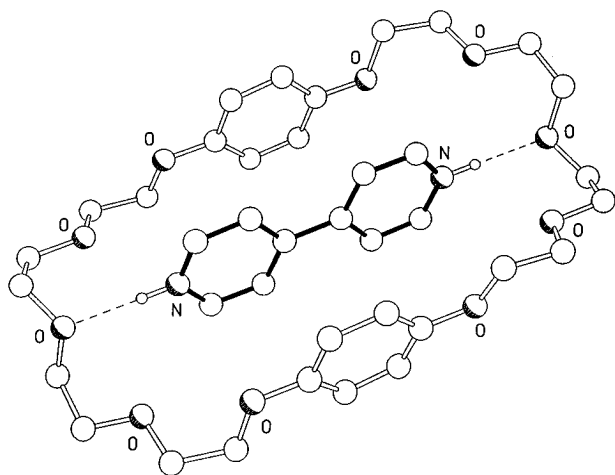

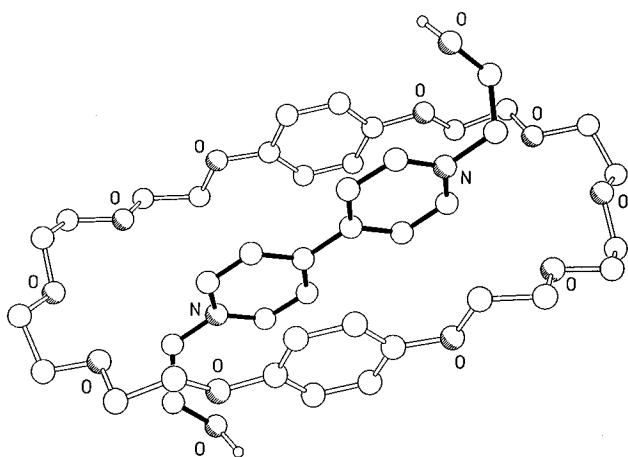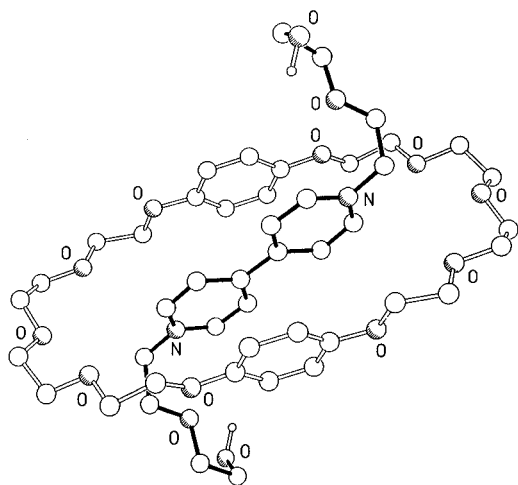**Figure 5.** Ball-and-stick representation of the supramolecular geometry adopted by the 1:1 complex [BPP34C10-BHEEBIPY][PF$_6$]$_2$ in the crystal.

In the case of [BPP34C10-BHEEBIPY][PF$_6$]$_2$, the BPP34C10 rings are aligned to form stacks (Figure 8) that extend in the crystallographic *b* direction, providing a continuous free pathway through which the dications are threaded. Inspection of the interthread contacts reveals the presence of significant [C−H···O] hydrogen bonding interactions between one of the β-bipyridinium hydrogen atoms in one thread and the hydroxyl hydrogen atoms of an adjacent thread and *vice versa* (the [C···O], [H···O]
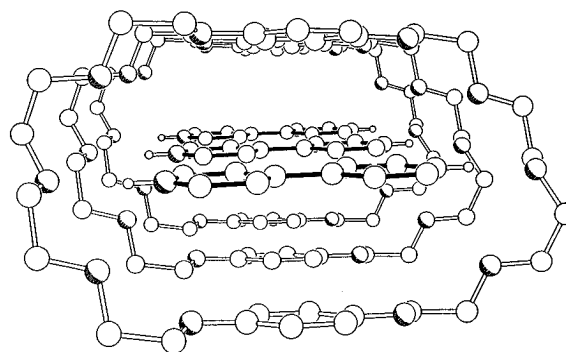

Figure 6. Ball-and-stick representation of one of the channel-like stacks adopted by the 1:1 complex [BPP34C10-BHBIPY][PF$_6$]$_2$ in the crystal.

Figure 7. Ball-and-stick representation of one of the pseudopolyrotaxane-like motifs adopted by the 1:1 complex [BPP34C10-BHEBIPY]-[PF$_6$]$_2$ in the crystal, showing the hydrogen bonding interactions between adjacent complexes and Me$_2$CO.

distances are 3.13, 2.24 Å and the [C−H···O] angle is 155°). The combined effects of these pairs of hydrogen bonds is to create a hydrogen bonded pseudopolyrotaxane structure similar to that observed for [BPP34C10-BHEBIPY][PF$_6$]$_2$ but without the requirement of an included solvent molecule element. Adjacent hydrogen bonded pseudorotaxane stacks pack with the hydroquinone rings within one stack aligned parallel and partially overlapping with those in the next. The interplanar ring−ring separation (3.63 Å) and the associated centroid−centroid separation (4.19 Å) are compatible with cooperative interstack π−π stabilizing interactions.

FABMS and ESMS. Fast atom bombardment mass spectrometry (FABMS) was employed for the characterization (Table 1) of the compounds having molecular weights up to approximately 3000 as well as for the characterization of the 1:1
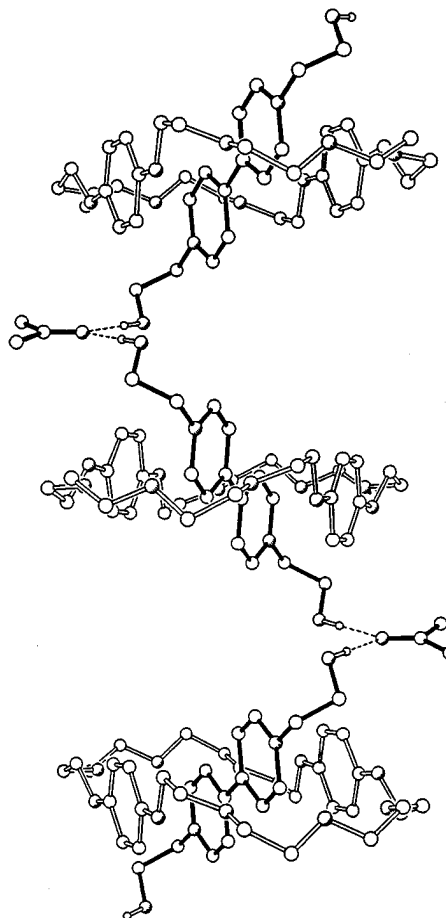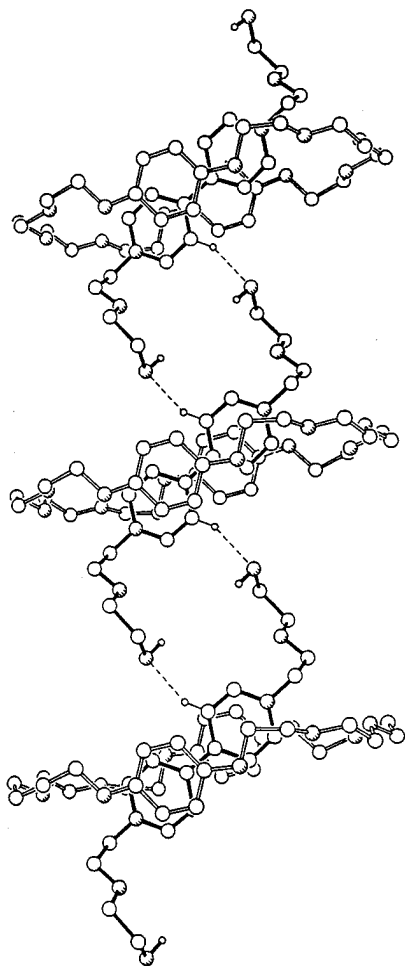
Figure 8. Ball-and-stick representation of one of the pseudopolyrotaxane-like motifs adopted by the 1:1 complex [BPP34C10-BHEEBIPY][PF$_6$]$_2$ in the crystal, showing the pairs of hydrogen bonding interactions occurring between adjacent complexes.

complexes [BPP34C10-BHBIPY][PF$_6$]$_2$, [BPP34C10-BHEBIPY][PF$_6$]$_2$, and [BPP34C10-BHEEBIPY][PF$_6$]$_2$. The rotaxanes with higher molecular weights were characterized (Table 2) by electrospray mass spectrometry (ESMS).

   Association Constants. The π-electron rich macrocycle BPP34C10 and the π-electron deficient paraquat bis(hexafluorophosphate) [PQT][PF$_6$]$_2$ form[2] a 1:1 adduct in solution. The bipyridinium unit of the guest [PQT][PF$_6$]$_2$ is sandwiched between the two hydroquinone rings of the macrocyclic host BPP34C10, affording a pseudorotaxane-like superstructure. Similarly, the bipyridinium-based guests [BHBIPY][PF$_6$]$_2$, [BHEBIPY][PF$_6$]$_2$, and [BHEEBIPY][PF$_6$]$_2$ are complexed[2d] by BPP34C10 with 1:1 stoichiometries. Upon combination of equimolar amounts of the host BPP34C10 and the π-electron deficient guests in acetone at ambient temperature, a deep orange color develops immediately as a result of the charge transfer interaction between the hydroquinone rings of the macrocycle and the bipyridinium unit of the guests. By employing the titration methodology[17] and following the charge-transfer band of the complexes by absorption spectroscopy in the visible region, the association constants and the binding energies of the 1:1 complexes have been evaluated. The association constants for the 1:1 complexes [BPP34C10-PQT][PF$_6$]$_2$, [BPP34C10-BHEBIPY][PF$_6$]$_2$, and [BPP34C10-BHEEBIPY]-[PF$_6$]$_2$ are very similar—730, 700, and 810 M^{-1}, respectively, ($\Delta G°$ *ca.* -3.9 kcal mol^{-1}), while the association constant for

(17) Connors, K. A. *Binding Constants*; Wiley: New York, 1987.

the 1:1 complex [BPP34C10-BHBIPY][PF$_6$]$_2$ is only 390 M^{-1}, presumably as a result of weaker π–π stacking interactions, as suggested by the X-ray crystal structure.

   ^{1}H NMR Spectroscopy. The ^{1}H NMR spectroscopic data in CD$_3$COCD$_3$ at ambient temperature for the 1:1 complexes between BPP34C10 and the bipyridinium-based, guests as well as for the related rotaxanes and reference compounds are listed in Table 3. In the case of the 1:1 adducts, exchange between the complexed and free species occurs rapidly on the ^{1}H NMR time scale at ambient temperature. Thus, the chemical shifts of the observed resonances are the averaged values between those for the free and complexed species. A significant upfield shift is observed for the protons of the guest in both the α- and β-positions with respect to the nitrogen atoms in the bipyridinium units. Similarly, upon complexation, the protons attached to the hydroquinone rings of BPP34C10 are shifted upfield by *ca.* 0.3 ppm. Interestingly, the 1:1 adduct [BPP34C10-BHBIPY][PF$_6$]$_2$ shows larger chemical shift differences in the protons of both the host and the guest, presumably as a result of a different complexation geometry. The ^{1}H NMR spectra of the [2]rotaxanes **8a**–**c** and **8e** show even higher chemical shift changes for the protons of both the macrocyclic and the dumbbell-shaped components. The protons in the α- and β-positions on the bipyridinium units are shifted upfield by *ca.* 0.3 and 0.5 ppm, respectively, while the hydroquinone ring protons are shifted upfield by 0.67 ppm. In the case of the [2]rotaxane incorporating two bipyridinium units within the dumbbell-shaped component **10a**, a chemical shift difference of only -0.14 and -0.26 ppm is observed for the protons in the α-positions and the β-positions, respectively, while the protons attached to the hydroquinone rings of the macrocyclic component are shifted upfield by 0.72 ppm. The ^{1}H NMR spectrum of the [3]rotaxane, incorporating two bipyridinium units within the dumbbell-shaped component **11a**, shows higher chemical shift differences for the protons in the α- and β-positions— -0.26 and -0.52 ppm, respectively—but almost the same upfield shift of 0.68 ppm for the hydroquinone ring protons. In the case of the [2]rotaxane incorporating three bipyridinium units within the dumbbell-shaped component **13c**, very small chemical shift differences are observed for the protons in the α- and β-positions— -0.10 and -0.16 ppm, respectively. However, the magnitude of the upfield shift for the hydroquinone ring protons is 0.70 ppm. The ^{1}H NMR spectra of the [3]rotaxane **14c** and [4]rotaxane **15c** incorporating three bipyridinium units within the dumbbell-shaped component **14c** and **15c** show increasingly higher chemical shift differences for the protons in the α- and β-positions— -0.17 and -0.30 ppm, respectively, for **14c**, and -0.29 and -0.51 ppm, respectively, for **15c**—but the upfield shift of the hydroquinone ring protons is once again only *ca.* 0.7 ppm. Thus, the chemical shift difference for the protons attached to the hydroquinone rings of the macrocycle is *ca.* -0.7 δ in the case of all the rotaxanes, while the chemical shift difference for the α- and β-protons is related approximately to the ratio of the number of bipyridinium recognition sites to the number of BPP34C10 macrocyclic units incorporated within the rotaxane structure. When all the bipyridinium recognition sites are "occupied" by the macrocyclic components, "saturation" values corresponding to *ca.* -0.3 and -0.5 ppm are observed for the α- and β-protons, respectively, independent of the total number of bipyridinium units. When free bipyridinium recognition sites are present, the macrocyclic component(s) is/are moving fast on the ^{1}H NMR time scale at ambient temperature from one recognition site to the other. Thus, the observed chemical shifts for the bipyridinium protons are averaged values between those of occupied

Table 1. FABMS Data[a,b] for the 1:1 Complexes [BPP34C10-BHBIPY][PF$_6$]$_2$, [BPP34C10-BHEBIPY][PF$_6$]$_2$, and [BPP34C10-BHEEBIPY]-[PF$_6$]$_2$, the Dumbbell-Shaped Compounds **7a−e**, **9a**, and **12c** as well as the Rotaxanes **8a−c**, **8e**, **10a**, **10e**, and **11a**

compound	M[c]	[M − PF$_6$]$^+$	[M − 2PF$_6$]$^+$	[M − 2PF$_6$-BPP34C10]$^+$
[BPP34C10-BHBIPY][PF$_6$]$_2$	(984)	839	694	
[BPP34C10-BHEBIPY][PF$_6$]$_2$	(1072)	927	782	
[BPP34C10-BHEEBIPY][PF$_6$]$_2$	(1160)	1015	870	
7a	(1698)		1408	
7b	(1726)		1436	
7c	(1754)		1464	
7d	(1782)		1492	
7e	(1810)		1520	
8a	(2234)		1944	1408
8b	(2262)	2117	1972	1436
8c	(2290)		2000	1464
8e	(2346)	2201	2056	1520
9a[d]	(2248)	2103	1958	
10a[d−f]	(2784)	2639	2494	1958
10e	(2896)		2606	
11a[d]	(3320)		3030	2494
12c[d−f]	(2854)	2709	2564	

[a] FABMS spectra were obtained with a Kratos MS80RF mass spectrometer coupled to a DS90 data system. The atom gun (Ion Tech Limited) was operated at 7 keV with a tube current of 2 mA. The primary beam of atoms was produced from research grade krypton. The samples were dissolved in a small amount of 3-nitrobenzyl alcohol (NOBA) or 2-nitrophenyloctyl ether (NPOE) that had been coated on to a stainless steel probe, and spectra were recorded in the positive-ion mode at a scan speed of 30 s per decade. [b] The measured masses correspond to the centroids of unresolved isotopic distributions. [c] The peaks corresponding to the molecular ions were not observed. The molecular weights are shown in parentheses. [d] A peak corresponding to the loss of three hexafluorophosphate counterions was observed. [e] A peak corresponding to the loss of one hexafluorophosphate counterion and one BPP34C10 macrocyclic component was observed. [f] A peak corresponding to the loss of three hexafluorophosphate counterions and one BPP34C10 macrocyclic component was observed.

Table 2. ESMS Data[a,b] for the Rotaxanes **11e**, **13c**, **14c**, **14e**, **15c**, and **15e**

rotaxane	M[c]	[M − 2PF$_6$]$^{2+}$	[M − 3PF$_6$]$^{3+}$	[M − 4PF$_6$]$^{4+}$
11e	(3432)	1571		
13c	(3390)	1550	985	702
14c	(3926)	1818	1164	837
14e	(3982)	1846		
15c	(4464)	2087	1343	
15e	(4520)	2115	1362	

[a] ESMS spectra were obtained using a VG Autospec triple focusing magnetic sector instrument operating at 4 KV accelerating voltage and fitted with an Electrospray ion source. Solvent delivery to the spraying capillary employed a Harvard Model 22 syringe pump operating at a flow rate of 3 μL min^{-1}. Solutions of samples (5−10 pmol μL^{-1} in MeCN) were introduced into the solvent flow *via* a Rheodyne model 7125 injection valve with a 20 μL loop. [b] The measured masses correspond to the centroids of unresolved isotopic distributions. [c] The peaks corresponding to the molecular ions were not observed. The molecular weights are shown in parentheses.

and "unoccupied" bipyridinium recognition sites and therefore the chemical shift differences are considerably lower than those attained when all the recognition sites are encircled by macrocyclic components, *i.e.*, saturation is reached.

The [2]rotaxane **10a** incorporates two bipyridinium recognition sites within the dumbbell-shaped component but only one BPP34C10 macrocycle. Thus, the macrocyclic component can move back and forth from one recognition site to the other, giving rise to a so-called molecular shuttle.[9,10] The equilibration (Table 4) between the two degenerate species is fast on the ^{1}H-NMR time scale in CD$_3$COCD$_3$ at 273 K. Thus, the ^{1}H-NMR spectrum of a CD$_3$COCD$_3$ solution of **10a** at this temperature shows[8b] (Figure 9) two sharp, well-resolved doublets for the two pairs of constitutionally heterotopic α-protons as well as two doublets for the two pairs of constitutionally heterotopic β-protons in the region between δ 8.0 and 10.0. On cooling the solution down, significant broadening of the resonances is observed, as a result of the decreased rate of the degenerate exchange process. At 233 K, the ^{1}H NMR spectrum shows a broad signal centered on δ 9.35 for all the α-protons and a second broad signal centered on δ 8.50 for all the β-protons. At 203 K, the shuttling process is slow on the ^{1}H NMR time

scale and the occupied and unoccupied bipyridinium recognition sites give distinct sets of resonances. Indeed, four resonances for the α-protons and four resonances for the β-protons are observed. By employing the coalescence method,[18] the free energy of activation ($\Delta G^{\ddagger}$) for the degenerate exchange process associated with the [2]rotaxane **10a** was calculated[8b] (Table 4) to be *ca.* 10 kcal mol^{-1}. Not surprisingly, the same temperature dependence of the ^{1}H NMR spectrum was observed for the [2]-rotaxane **10e**, and the same value for the free energy of activation of the process was obtained.[7] This observation suggests that the mechanisms of the dynamic processes are similar in both cases.

Kinetic Studies. The slipping approach to the synthesis of rotaxanes is based upon the size complementarity between the macrocyclic component BPP34C10 and the tetraarylmethane-based stoppers. By employing an appropriate amount of thermal energy, the macrocyclic component can be induced to slip over the stoppers, and the noncovalent bonding interactions with the bipyridinium recognition sites then provide a thermodynamic trap (Figure 2) for the macrocycle, thus raising the energy of activation for the dethreading—extrusion—process. However, the process is a reversible one and, by employing much higher temperatures, the extrusion of the macrocyclic component can indeed be achieved, affording the free dumbbell-shaped component and BPP34C10. On heating solutions of the rotaxanes in CD$_3$SOCD$_3$ at 100 °C, complete extrusion of the macrocyclic component can also be accomplished. The chemical shifts of the resonances, arising from the rotaxanes and the corresponding free dumbbell-shaped components, are significantly different in the ^{1}H NMR spectra and so the extrusion processes can be monitored easily by the integration of the appropriate resonances.
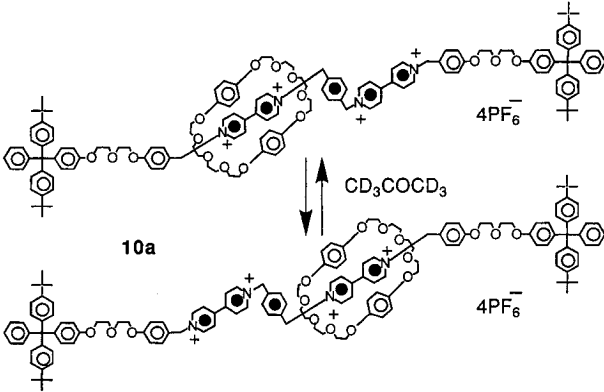
The extrusion process associated with the [3]rotaxane **11a** is illustrated in Table 5. The loss of the first BPP34C10 macrocycle affords the [2]rotaxane **10a** and subsequent loss of the second BPP34C10 macrocycle yields the free dumbbell-shaped compound **9a**. The partial ^{1}H NMR spectra of a CD$_3$-

(18) (a) Sutherland, I. O. *Ann. Rep. NMR Spectrosc.* **1971**, *4*, 71−235. (b) Sandström, J. *Dynamic NMR Spectroscopy*; Academic Press: London, 1982.

Table 3. ^{1}H NMR Data [δ Values (Δδ Values)] in CD$_3$COCD$_3$ at Ambient Temperature for the 1:1 Complexes, the Dumbbell-Shaped Derivatives, and the Rotaxanes

compound	α-CH[a] [δ (Δδ)]	β-CH[b] [δ (Δδ)]	ArH[c] [δ (Δδ)]
BPP34C10			6.77
[PQT][PF$_6$]$_2$	9.36	8.83	
[BPP34C10-PQT][PF$_6$]$_2$	9.19 (−0.17)	8.42 (−0.41)	6.38 (−0.39)
[BHBIPY][PF$_6$]$_2$	9.44	8.85	
[BPP34C10-BHBIPY][PF$_6$]$_2$	9.10 (−0.34)	8.12 (−0.73)	6.38 (−0.39)
[BHEBIPY][PF$_6$]$_2$	9.39	8.85	
[BPP34C10-BHEBIPY][PF$_6$]$_2$	9.24 (−0.15)	8.53 (−0.32)	6.46 (−0.31)
[BHEEBIPY][PF$_6$]$_2$	9.43	8.83	
[BPP34C10-BHEEBIPY][PF$_6$]$_2$	9.24 (−0.19)	8.43 (−0.40)	6.44 (−0.33)
7a	9.50	8.83	
8a	9.19 (−0.31)	8.27 (−0.56)	6.10 (−0.67)
7b	9.48	8.81	
8b	9.18 (−0.30)	8.27 (−0.54)	6.10 (−0.67)
7c	9.45	8.78	
8c	9.19 (−0.26)	8.28 (−0.50)	6.10 (−0.67)
7e	9.46	8.79	
8e	9.19 (−0.27)	8.28 (−0.51)	6.10 (−0.67)
9a	9.44	8.76	
10a	9.30 (−0.14)	8.45 (−0.31)	6.05 (−0.72)
11a	9.18 (−0.26)	8.24 (−0.52)	6.09 (−0.68)
12c	9.46	8.76	
13c	9.36 (−0.10)	8.60 (−0.16)	6.07 (−0.70)
14c	9.29 (−0.17)	8.44 (−0.30)	6.08 (−0.69)
15c	9.17 (−0.29)	8.25 (−0.51)	6.08 (−0.69)

[a] Chemical shifts (δ) and chemical shift differences (Δδ) for the protons in the α-positions with respect to the nitrogen atoms on the bipyridinium units. [b] Chemical shifts (δ) and chemical shift differences (Δδ) for the protons in the β-positions with respect to the nitrogen atoms on the bipyridinium units. [c] Chemical shifts (δ) and chemical shift differences (Δδ) for the protons attached to the hydroquinone rings incorporated within the BPP34C10 macrocycle.

Table 4. Kinetic and Thermodynamic Parameters for the Degenerate Site Exchange Process Associated with the [2]Rotaxane **10a** in CD$_3$COCD$_3$

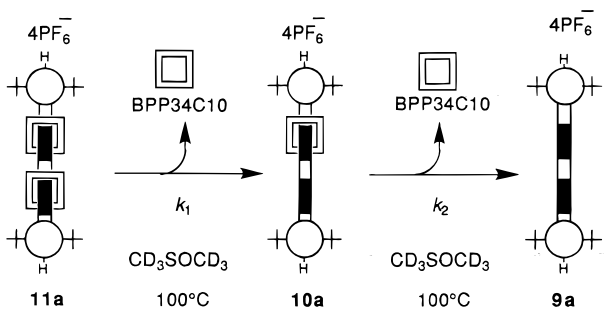| probe protons[a]	Δν[b] (Hz)	k_c[c] (s^{-1})	T_c[d] (K)	ΔG‡[e] (kcal mol^{-1})
α-CH	152	337.6	214.6	9.9
β-CH	112	248.8	214.6	10.0

[a] The protons in the α-positions and in the β-positions with respect to the nitrogen atoms on the bipyridinium units were employed as the probe protons. [b] Limiting frequency separation (Δν) between the coalescing resonances. [c] Rate constant (k_c) at the coalescence temperature (T_c) for the degenerate site exchange process calculated from the expression $k_c = \pi(\Delta\nu)/2^{1/2}$. [d] Temperature of the spectrometer probe at coalescence. [e] Free energy barrier (ΔG‡) for the degenerate site exchange process calculated employing the Eyring equation.

SOCD$_3$ solution of the [3]rotaxane **11a** are depicted in Figure 10. The partial ^{1}H NMR spectrum at 25 °C, shows the resonances corresponding to the protons in the α- and β-positions with respect to the nitrogen atoms in the bipyridinium units of the [3]rotaxane **11a** only. On heating the solution up to 100 °C, the macrocyclic component starts to be extruded, and the partial ^{1}H NMR spectrum recorded at 100 °C after 3 min shows the appearance at lower fields of the resonances corresponding
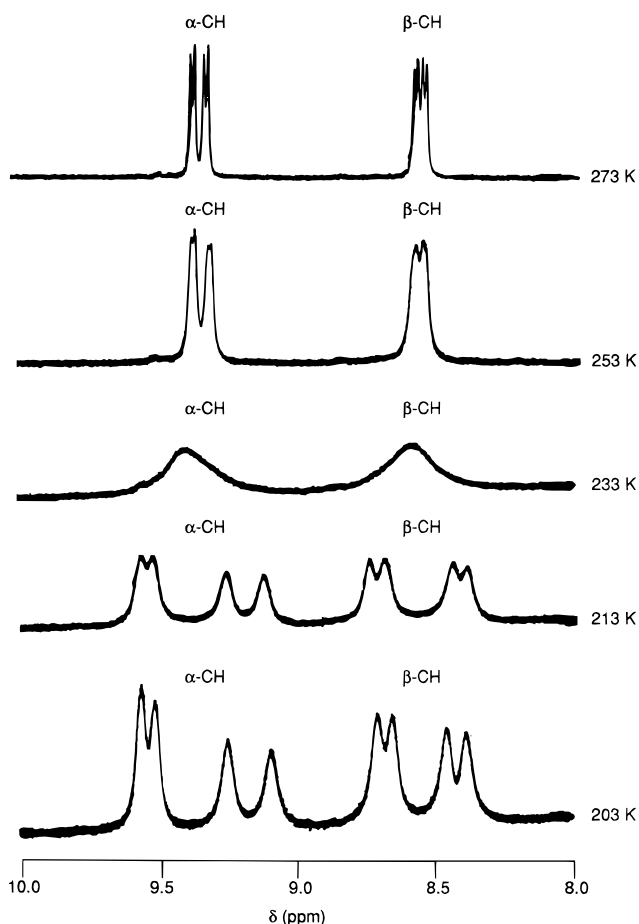
Figure 9. Partial variable temperature ^{1}H NMR spectra of a CD$_3$-COCD$_3$ solution of the [2]rotaxane **10a**.

to the α- and β-protons of the [2]rotaxane **10a**. After 10 min, a third set of resonances, corresponding to the α-protons and β-protons of the free dumbbell-shaped compound **9a**, can be

Self-Assembly of [n]Rotaxanes

J. Am. Chem. Soc., Vol. 118, No. 21, 1996 4941

Table 5. First Order Rate Constants Derived[a] for the Conversion of the [3]Rotaxane **11a** to the [2]Rotaxane **10a** (k_1) and subsequently for the Conversion of the [2]Rotaxane **10a** to the Dumbbell-Shaped Compound **9a** (k_2) in CD_3SOCD_3 at 100 °C

	α-CH[b]	β-CH[c]
$k_1 (\times 10^{-4}\,s^{-1})$	18.90 ± 0.80	20.30 ± 0.60
$k_2 (\times 10^{-4}\,s^{-1})$	4.91 ± 0.68	4.92 ± 0.61

[a] Concentration data were obtained from integration of the appropriate signals in the ^{1}H NMR spectrum recorded at 100 °C in CD_3SOCD_3 recorded at appropriate time intevals. The concentration data were then fitted to eqs 1, 2, and 3 using the program DeltaGraph Pro 3 (Version 3.0.1, DeltaPoint Inc., 1993) running on a Apple Macintosh Quadra 650 microcomputer. [b] The values in this column were derived from data obtained using the integration of the resonances corresponding to the protons α to the nitrogen atoms on the bipyridinium units. [c] The values in this column were derived from data obtained using the integration of the resonances corresponding to the protons β to the nitrogen atoms on the bipyridinium units.
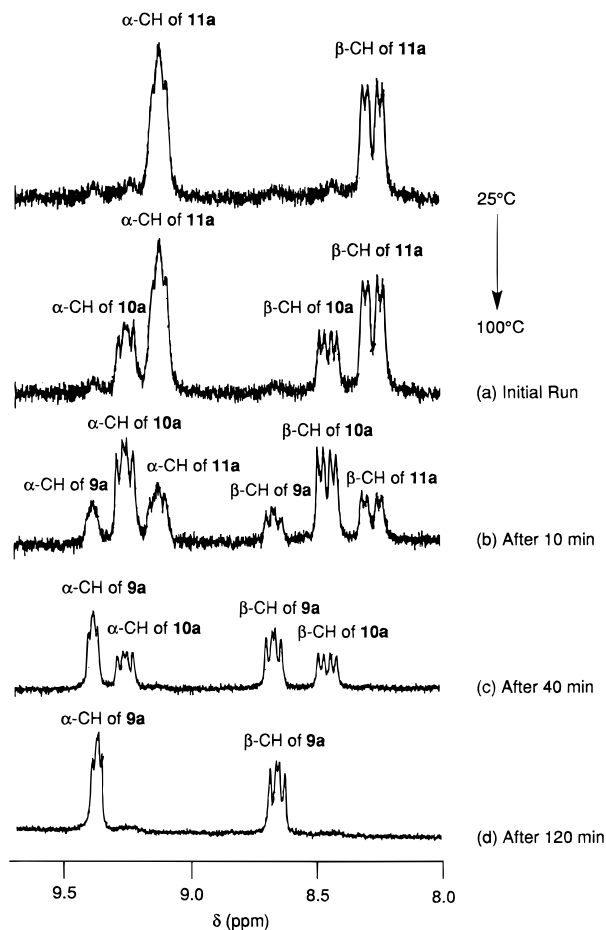
Figure 10. Partial ^{1}H NMR spectra of a CD_3SOCD_3 solution of the [3]rotaxane **11a** illustrating the extrusion process associated with **11a**.

observed at even lower fields. The partial ^{1}H NMR spectrum, recorded after 120 min, shows only the resonances of the free
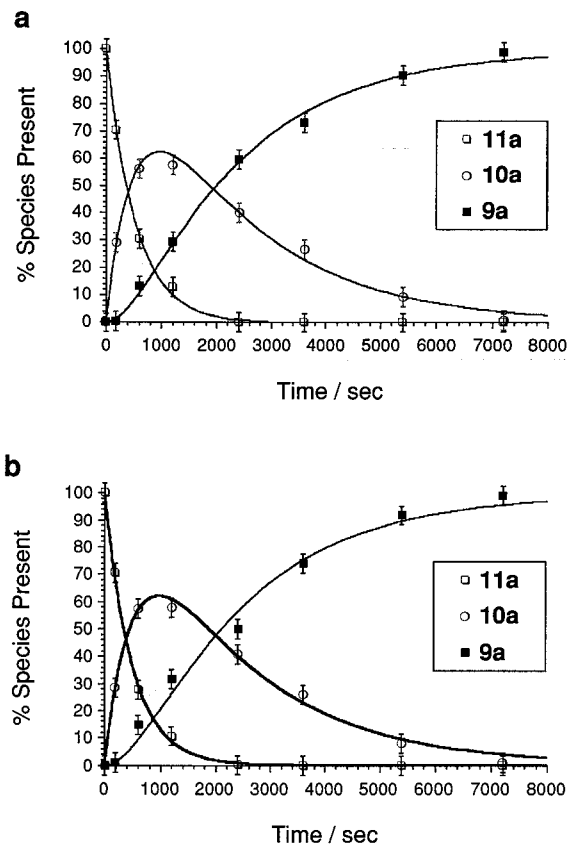
Figure 11. Nonlinear curve fitting of the eqs 1−3 to the concentration data derived from ^{1}H NMR spectroscopy following the integration of the resonances corresponding to (a) the α-protons and (b) the β-protons.

dummbell-shaped compound **9a**, demonstrating the successful completion of the extrusion process.

A nonlinear curve fitting method[19] was used to fit (Figure 11) eqs 1, 2, and 3 to the concentration data derived from the ^{1}H NMR spectroscopic experiments already described.

$$[\mathbf{11a}] = [\mathbf{11a}]_0 e^{-k_1 t} \tag{1}$$

$$[\mathbf{10a}] = \frac{[\mathbf{11a}]_0 k_1}{k_2 - k_1}(e^{-k_1 t} - e^{-k_2 t}) \tag{2}$$

$$[\mathbf{9a}] = [\mathbf{11a}]_0 \left[1 + \frac{1}{k_1 - k_2}(k_2 e^{-k_1 t} - k_1 e^{-k_2 t})\right] \tag{3}$$

This procedure was performed using data for both the α- and β-bipyridinium proton resonances: it afforded the values for k_1 and k_2 shown in Table 5.

From these results, it appears that the initial loss of one BPP34C10 ring from the [3]rotaxane **11a** is significantly faster—indeed, by a factor of approximately four—than the loss of the BPP34C10 ring from the [2]rotaxane **10a**. This difference is almost certainly the result of the fact that there are two recognition sites per BPP34C10 ring in **10a**, compared with only one site per BPP34C10 ring in **11a**. The increased number of bipyridinium recognition sites is clearly associated with a larger thermodynamic trap and a consequently higher activation energy for the extrusion of a crown ether from **10a** than from **11a**. Indeed, when the extrusion experiment was repeated, starting from the [2]rotaxane **8a**, which incorporates only one bipyridinium recognition site, the extrusion process proceeds at a rate

(19) In the analysis described, only the forward reactions are considered. However, inclusion of the reverse reactions for the two kinetic steps has no significant effect on the values of the rate constants k_1 and k_2 obtained.

**Table 6.** Pseudo Second Order Rate Constants for the Formation[a] of the [2]Rotaxane **8a−d** by Slipping

	rate constant [10^{-7} M^{-1} s^{-1}]						
compound[b]	298 K	303 K	310 K	317 K	323 K	328 K	333 K
7a	1.65	3.16	4.66	8.12	9.86	12.1	13.1
7b	1.75	2.91	4.88	6.35	8.38	10.2	11.3
7c	nd	2.82	4.70	6.50	8.57	10.5	11.7
7d	nd	nd	nd	nd	nd	nd	1.66

[a] The processes were followed by UV−vis spectroscopy by monitoring the change of the intensity of the charge transfer band associated with the [2]rotaxanes by means of a computer-controlled Perkin Elmer Lambda 2 spectrophotometer fitted with a thermostatic temperature controller. [b] Starting dumbbell-shaped compound employed for the formation of the [2]rotaxanes after slipping of BPP34C10.

similar to that for the conversion of **11a** into **10a**. When the extrusion experiment is performed with the [2]rotaxane **10a**, incorporating two bipyridinium recognition sites, the extrusion of the macrocycle is much slower and the calculated first order rate constant is similar to that obtained (k_2) for the same process in the extrusion experiment involving **11a**.

When the same experiment was repeated with the [2]rotaxanes **8e** and **10e** and the [3]rotaxane **11e** incorporating the "*t*-Bu-substituted" stoppers, no extrusion was observed during 150 min. The tris(4-*tert*-butylphenyl)methyl-based stoppers are too bulky for the passage of the BPP34C10 macrocycle over them, and thus, neither the "slipping-on" nor the "extrusion-from" can be achieved when the *t*-Bu-substituted stoppers and BPP34C10 are employed. In order to illustrate the point at which the stoppers become too large to permit the passage of BPP34C10 over them, the apparent second order rate constants for the formation of the [2]rotaxanes **8a−c** by the slipping approach are listed in Table 6. The rate constants were derived over a range of temperatures, using absorption UV−vis spectroscopy to follow the change in intensity of the charge-transfer absorption band of the [2]rotaxane, arising from the interaction between the hydroquinone rings of the macrocycle and the bipyridinium recognition sites incorporated within the dumbbell-shaped components. No significant differences in the apparent rate constants at a range of different temperatures were observed for the formation of the [2]rotaxanes **8a−c**. Thus, it would appear that an almost identical steric barrier is imposed to the slipping of the BPP34C10 macrocycle by the three different "H-substituted", "Me-substituted", and "Et-substituted" stoppers. However, when the dumbbell-shaped compound **7d** incorporating the "*i*-Pr-substituted" stopper units is employed, the rate of formation at 333 K of the corresponding [2]rotaxane is approximately one order of magnitude smaller than the rates of formation of the [2]rotaxane **8a−c**. Thus, the barrier for the slipping of the BPP34C10 macrocycle over 4-alkylphenyl-bis-(4-*tert*-butylphenyl)methyl-based stoppers is reached on going from the Et-substituted to the *i*-Pr-substituted stoppers. These results were confirmed by the preparative experiments illustrated in Scheme 8. The [2]rotaxanes **8a−c** were self-assembled in 52, 45, and 47% yield, respectively, by means of a slipping procedure. However, when the *i*-Pr-substituted dumbbell-shaped compound **7d** was employed under otherwise identical conditions, no rotaxane was isolated.

Absorption and Luminescence Properties. The rotaxanes examined in this paper are particularly interesting molecular compounds from the vantage point of electronic absorption and luminescence properties since they contain a number of different chromophoric components. Some of these components are relatively isolated, whereas others interact more or less strongly. Comparison between the properties of suitable model compounds of each component and the properties of the dumbbell-
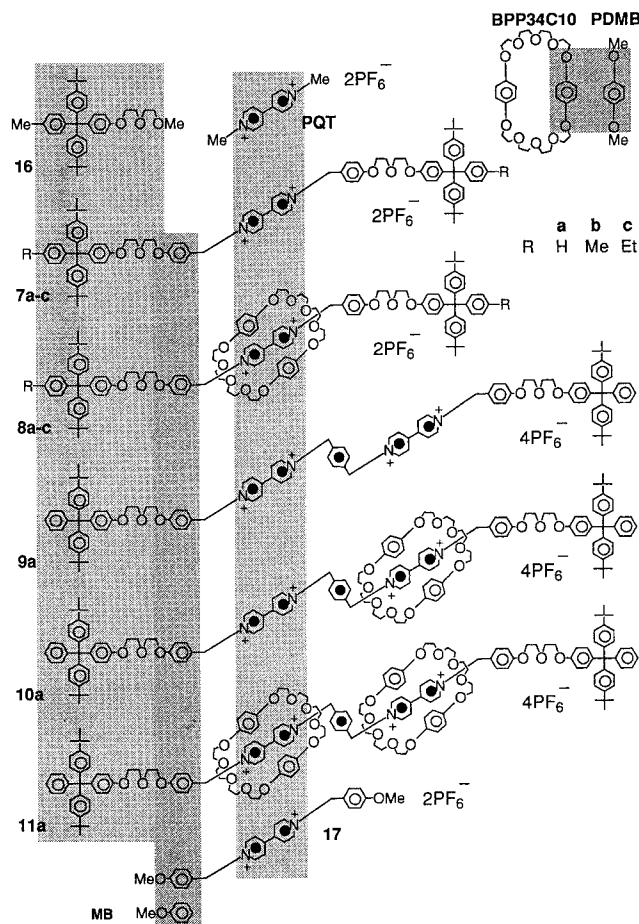
Figure 12. Chromophoric and electroactive units that can be singled out in the dumbbell-shaped compounds **7a−c** and **9a**, and in the rotaxanes **8a−c, 10a,** and **11a**.

shaped compounds, macrocycle, and rotaxanes reveals the degree of intercomponent interaction. The chromophoric units that can be singled out in the compounds that have been examined are of the following types (Figure 12): methoxybenzene (MB), *p*-dimethoxybenzene (PDMB), the tetraarylmethane-based derivative **16**, and paraquat (PQT). For example, the [3]rotaxane **11a** is made up of two BPP34C10 macrocycles and the dumbbell-shaped component **9a**; in its turn, each BPP34C10 macrocycle is made of two PDMB-like chromophoric units, and the dumbbell-shaped component **9a** contains six chromophoric units, namely, two **16**-like residues that play the role of the stoppers, two MB-like units, and two PQT-like units.

A. Chromophoric Units. The absorption and emission spectra of the model compounds MB, PDMB, PQT, and **16** in MeCN at room temperature are shown in Figure 13 and the most relevant data are collected in Table 7. It is obvious that none of these compounds shows absorption bands above 310 nm. MB, PDMB, and **16** exhibit a strong fluorescence band in the 280−360 nm spectral range, and a phosphorescence band (in butyronitrile rigid matrix at 77 K) with $\lambda_{max} = 384$ nm ($\tau = 3.0$ s), 408 nm ($\tau = 2.1$ s), and 403 nm ($\tau = 2.3$ s), respectively. PQT does not show any luminescence.

B. Macrocycle BPP34C10, Thread 17, and Dumbbell-Shaped Compounds 7a−c and 9a. As previously observed,[20] the absorption spectrum of the BPP34C10 macrocycle in MeCN

(20) Anelli, P. L.; Ashton, P. R.; Ballardini, R.; Balzani, V.; Delgado, M.; Gandolfi, M. T.; Goodnow, T. T.; Kaifer, A. E.; Philp, D.; Pietraszkiewicz, M.; Prodi, L.; Reddington, M. V.; Slawin, A. M. Z.; Spencer, N.; Stoddart, J. F.; Vicent, C.; Williams, D. J. *J. Am. Chem. Soc.* **1992**, *114*, 193−218.
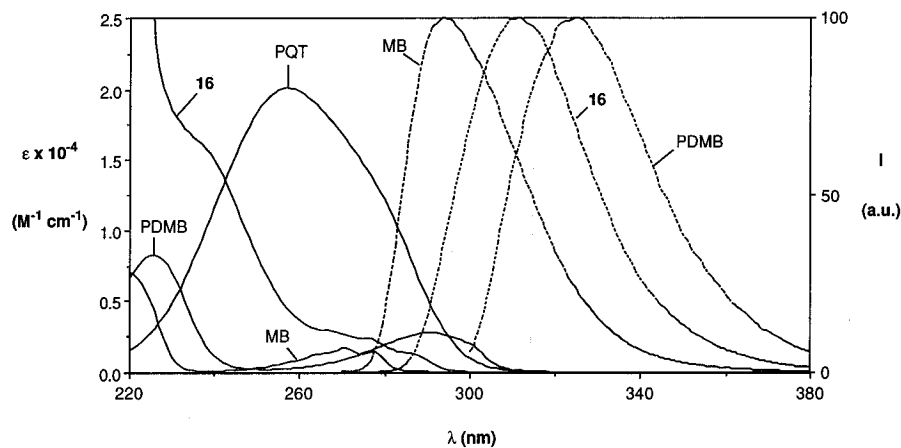
Self-Assembly of [n]Rotaxanes

J. Am. Chem. Soc., Vol. 118, No. 21, 1996 4943

Figure 13. Absorption (full lines) and emission (dashed lines) spectra of the model compounds MB, PDMB, PQT, and **16** in MeCN solution at room temperature.

Table 7. Absorption and Emission Properties in Acetonitrile Solution at Room Temperature

compound	absorption[a]		fluorescence		
	λ (nm)	ϵ (M^{-1} cm^{-1})	λ (nm)	τ^b (ns)	ϕ^c
PQT	260	20000			
MB	277	1400	293	5.0	0.10
PDMB	290	2800	320	2.5	0.11
16	270	2600	314	4.5	0.08
BPP34C10	290	5200	320	2.5	0.08
17	336	1300			
7b[d]	336	1100	314	0.4[e]	9×10^{-3}
8b[f]	450	500	314	≤0.5	9×10^{-3}
9a	240	61800	314	≤0.5	3×10^{-3}
	340sh	1400			
10a	262	54000	317	≤0.5	g
	455	550			
11a	262	53000	320	≤0.5	g
	460	1050			

[a] Lowest energy absorption band. [b] Lifetime of the fluorescent excited state measured with the single photon counting equipment, unless otherwise noted. [c] Fluorescence quantum yield. [d] Compounds **7a** and **7c** exhibit the same behavior as **7b**. [e] Measured with a picosecond instrument (see experimental). [f] [2]Rotaxanes **8a** and **8c** exhibit the same behavior as **8b**. [g] Not measured.

has the shape expected for two PDMB units, but it is less intense; its fluorescence spectrum is identical to that of PDMB, except for a lower (*ca.* 30%) intensity. In rigid matrix at 77 K, its phosphorescence band is very similar to that exhibited by PDMB. The dumbbell-shaped compounds described in this investigation contain a large number of chromophoric units. In an attempt to interpret better their spectroscopic properties, we have prepared and examined compound **17** (Figure 12), which is the central component of the dumbbell-shaped compounds **7a**−**c**. Such a component is particularly interesting since it is made up of a PQT-like electron-acceptor unit and two MB-like electron-donor units. One might therefore expect the presence of charge-transfer bands in the absorption spectrum of **17**. This is indeed the case, as shown in Figure 14. Of particular interest for the following discussion is the broad and weak band of **17** in the near UV region (λ_{max} = 336 nm). The charge-transfer (CT) character of this band is proved by the fact that the absorption maximum is displaced on changing solvent polarity (364 nm in CH_2Cl_2). This band will be hereafter called CT-(*intra*) in order to distinguish it from other CT bands (*vide infra*). The presence of a CT(*intra*) excited state below the lowest spin-allowed excited state (S$_1$) of the methoxybenzene units of **17** has important consequences on the emission properties, since such a state introduces a fast radiationless deactivation route for S$_1$ (Figure 15, top right-hand corner), thereby preventing
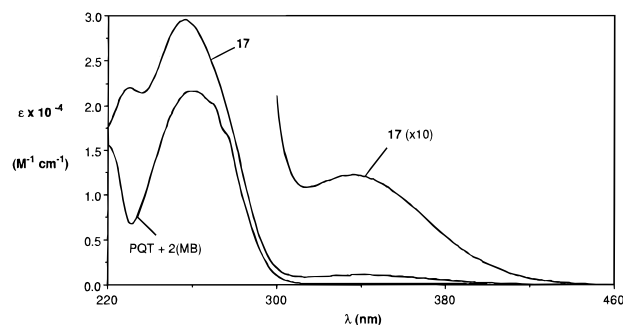

Figure 14. Absorption spectrum in MeCN solution at room temperature of compound **17** compared with the sum of the absorption spectra of its separated components.

its fluorescence. In a rigid matrix at 77 K, not only the fluorescence band but also the phosphorescence band of the methoxybenzene units disappear.

The absorption spectrum of the dumbbell-shaped compound **7b** is almost identical to that shown by a 1:2 mixture of **17** and **16** (Figure 16). This observation demonstrates that the two stoppers and the central component of the dumbbell-shaped compound interact, as expected, only very weakly, because of the relatively long separation distance. Therefore, in the spectrum of the dumbbell-shaped compound **7b** as well as in that of the analogous compounds **7a** and **7c** one can clearly observe the CT(*intra*) band at 336 nm, characteristic of the central component **17**. As it happens, for **17**, the maximum of this band moves to lower energy in going from MeCN to CH_2-Cl_2. Although weak, the electronic interaction between the stoppers and the central component in the dumbbell-shaped compounds **7a**−**c** is not without consequences for the emission properties. The fluorescence intensity and lifetime of the stopper chromophoric units **16** in the dumbbell-shaped compound **7b** (Table 7) are, in fact, reduced by approximately 10 times, owing to the presence of the central component, indicating the occurrence of a fast (*ca.* 2×10^9 s^{-1}) energy- (Figure 15, bottom) or electron-transfer quenching process.[21] At 77 K, no phosphorescence can be observed. The absorption and luminescence properties (Table 7) of the dumbbell-shaped compound **9a**, which contains the same chromophoric units as **7a**, confirm that the intercomponent electronic interactions are very weak.

C. Rotaxanes. The absorption spectrum of the [2]rotaxane **8b** is shown in Figure 17, where the sum of the spectra of its two separated components—namely, the BPP34C10 macrocycle

(21) The rate constant of the quenching process is obtained by the equation $1/\tau - 1/\tau°$, where τ and $\tau°$ are the lifetime of the fluorescence of the stoppers unit in **7a** and of the model compound **16**, respectively.
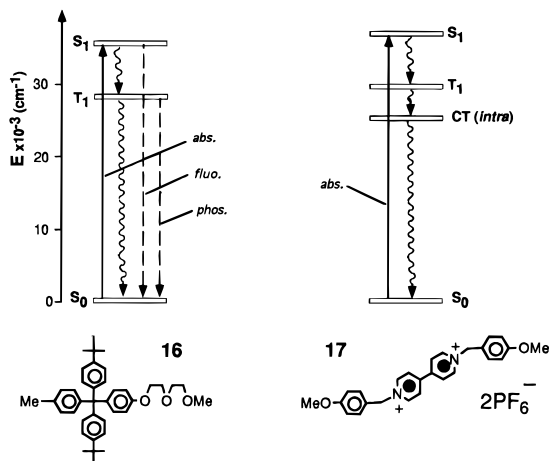
Figure 15. Schematic energy-level diagrams for the dumbbell-shaped compounds **7a**−**c** (bottom) and for the model compounds (top). The energy levels of the S_1 and T_1 excited states have been evaluated from the onset of the emission spectra, and the energy level of the CT(*intra*) excited state has been approximately taken as the energy at which the CT(*intra*) absorption band has 10% of its maximum intensity.
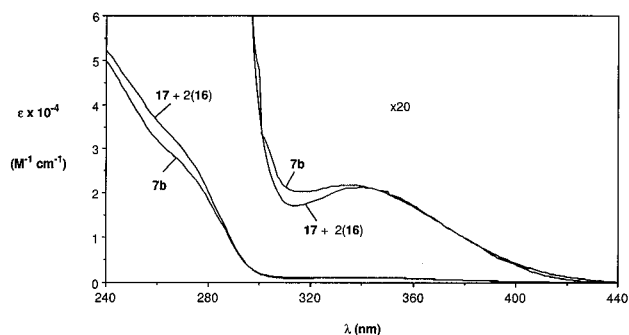

Figure 16. Absorption spectrum in MeCN solution at room temperature of the dumbbell-shaped compound **7b** compared with the sum of the absorption spectra of the reference compounds.

and the dumbbell-shaped compound **7b**—are also shown for comparison purposes. In **8b**, the 336 nm band of its dumbbell-shaped component is covered by a high intensity tail and a new broad absorption band, with a maximum around 450 nm, is present. On going from MeCN to CH_2Cl_2, the band maximum is displaced, as expected for a charge-transfer band. By analogy with the behavior of a [2]rotaxane containing a hydroquinone unit in the dumbbell-shaped component and two bipyridinium units in the cyclophane,[20] the band with a maximum at 450 nm can be assigned to a charge-transfer transition involving the
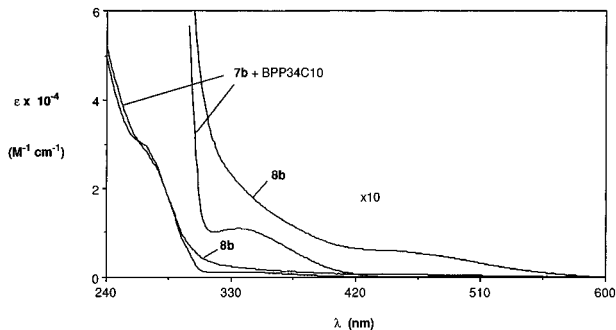

Figure 17. Absorption spectrum in MeCN solution at room temperature of the [2]rotaxane **8b** compared with the sum of the absorption spectra of the the reference compounds.

p-dimethoxybenzene units of the BPP34C10 macrocycle as the donors and the bipyridinium unit of the dumbbell **7b** as an acceptor. Such a band, and the corresponding electronic transition, are indicated hereafter by CT(*inter*) to avoid confusion with the above discussed CT(*intra*) found in the *free* **7a**−**c** compounds.

As far as luminescence is concerned, the spectrum of the [2]-rotaxane **8b** differs (Table 7) strongly from the sum of the spectra of its two separated components, BPP34C10 and **7b**. Upon excitation at 230 nm, in the case of the rotaxane the emission band of the stopper units (λ_{max} = 314 nm) has practically the same intensity as in the mixture of the two components, whereas the emission band of the BPP34C10 macrocycle (λ_{exc} = 280 nm) is no longer present. This result can be accounted for by the charge-transfer interaction—already identified in the absorption spectrum—between the macrocycle and the bipyridinium unit of the dumbbell. In fact, the CT-(*inter*) excited state lies below the fluorescent level of BPP34C10 and, therefore, offers a fast radiationless deactivation route (Figure 18). By contrast, the fluorescent level of the stopper units, which is already partially quenched *via* the CT(*intra*) excited state of the dumbbell-shaped component **7b**, does not seem to be further quenched by the presence of the CT(*inter*) level. At 77 K, no phosphorescence is observed. The behavior of [2]rotaxanes **8a** and **8c** is identical to that of **8b**. The energy-level diagram for [2]rotaxanes **8a**−**c**, obtained by combining the energy levels of dumbbell-shaped **7a**−**c** and BPP34C10 components, and including the CT(*inter*) excited state, is illustrated schematically in Figure 18. The [2]rotaxane **10a** differs from **8a** because of the additional presence of a second bipyridinium recognition site in its dumbbell-shaped component, separated from the first bipyridinium recognition site by a *p*-xylene spacer (Figure 12). The absorption spectrum and fluorescence properties of **10a** are, as expected, very similar to those of **8a**. The [3]rotaxane **11a** differs from **10a** because of the additional presence of a second BPP34C10 macrocycle (Figure 12). In this compound, it is expected that each bipyridinium recognition site is encircled by a BPP34C10 macrocycle, giving rise to a CT(*inter*) absorption band at the same wavelength as that found for **10a**, but twice as intense. This expectation is fulfilled, as one can see from the data reported in Table 7. The luminescence properties are identical to those shown by **10a.** Higher rotaxanes have not been investigated since, on the basis of the above results, they are not expected to exhibit any further special spectroscopic and excited-state feature.

Electrochemistry. As in the case of the spectroscopic properties, it is convenient to discuss the electrochemical properties of the dumbbell-shaped compounds and rotaxanes by comparison with the properties of the isolated components (Figure 12). The electrochemical properties of the redox active
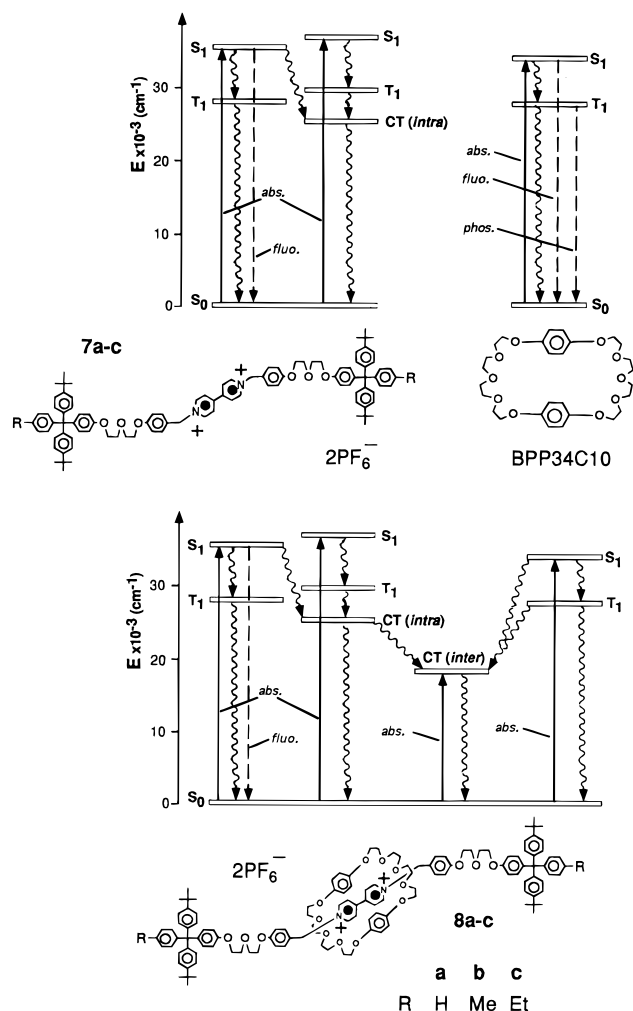
Figure 18. Schematic energy-level diagrams for the [2]rotaxanes **8a−c** (bottom) and for the *free* **BPP34C10** macrocycle and dumbbell-shaped components **7a−c** (top). Energy levels evaluated as specified in caption to Figure 15.

Table 8. Electrochemical Results in Argon-Purged Acetonitrile Solution at Room Temperature[a]

compd	reduction				oxidation
MB[b]					+1.8
PDMB[c]					+1.3
PQT[c]	−0.43		−0.84		
16					+1.5
BPP34C10[c]					+1.3
17	−0.37		−0.80		>+2.0
7a−c	−0.37		−0.80		+1.5
8a−c	−0.47		−0.87		+1.4
9a	−0.33[d]		−0.78[d]		+1.5
10a	−0.33	−0.44	−0.77	−0.86	+1.4
11a	−0.44[d]		−0.85[d]		+1.4

[a] Potentials in volts vs SCE; the reduction processes are reversible (E1/2 values reported) and, unless otherwise noted, monoelectronic; all the oxidation processes observed are irreversible (only the first potential value, evaluated from the DPV peaks, is reported). [b] See ref 22. [c] See ref 20. [d] Bielectronic wave.

compounds MB, PDMB, **16**, and PQT, the macrocycle BPP34C10, the thread **17**, the dumbbell-shaped compounds **7a−c** and **9a**, the [2]rotaxanes **8a−c** and **10a**, and the [3]-rotaxane **11a** are summarized in Table 8. The reduction processes, which involve the bipyridinium units, are reversible and can therefore be correlated and interpreted. The oxidation processes are of much less quantitative value because they are irreversible.

A. Redox Active Units. The redox properties of the compounds MB,[22] PDMB,[20] and PQT[20] have been reported in the literature. As expected on the basis of simple substituent effects, the first oxidation process of compound **16** occurs at a potential less positive than MB, but more positive than PDMB (Table 8).

B. Macrocycle BPP34C10, Thread 17, and Dumbbell-Shaped Compounds 7a−c and 9a. As previously reported,[20] in the BPP34C10 macrocycle the two *p*-dimethoxybenzene-like units are oxidized at distinct potentials. The first oxidation process practically coincides with that of PDMB, whereas the second one is displaced to a slightly more positive potential (+1.37 V, *vs* SCE). In the thread-like compound **17**, which constitutes the central part of the dumbbell-shaped compounds **7a−c**, the first and second reductions of the bipyridinium unit occur at less negative potential values than PQT, because of the presence of an electron-donor substituent (Table 8). For the same reason, oxidation of the methoxybenzene-like units of **17** is deflected to more positive potentials (outside the potential window of the solvent used) compared with MB (Table 8). The dumbbell-shaped compound **7a** behaves exactly as expected on the basis of its **16**-like stoppers and **17**-like central part, indicating that there is no substantial electronic interaction between the redox active centers. This result is not in disagreement with the quenching of the stopper luminescence (*vide supra*), since an electronic interaction of less than 0.01 eV—not sizeable in electrochemical experiments—is large enough to cause fast intercomponent energy- and electron-transfer processes.[23] The electrochemical behavior of compounds **7b** and **7c** is, as expected, identical to that of compound **7a**. The dumbbell-shaped compound **9a** is made of two **16**-like stoppers and a central part that contains two bipyridinium-type units separated by a *p*-xylene spacer. The oxidation behavior is the same as for **16**, indicating again that the stoppers are isolated from the electrochemical viewpoint. On reduction, two two-electron waves are observed (Table 8), showing also that the two bipyridinium units of the central component are electronically uncoupled. The lower reduction potential values of the bipyridinium units of **9a**, compared with those of the bipyridinium unit of **7a−c**, can be attributed to the phenylene spacer in **9a**.

C. Rotaxanes. In the potential window examined, the [2]-rotaxanes **8a**, **8b**, and **8c** show identical behavior, *i.e.*, two reduction and more than two oxidation waves (Table 8). The two reduction waves can easily be assigned to the first and second reduction process of the bipyridinium unit present in the dumbbell-shaped components **7a−c**. One notices that both waves are displaced to more negative potentials because, in the rotaxane, the bipyridinium unit is engaged in a charge transfer interaction with the electron donating macrocycle. As expected, the displacement of the first reduction wave (100 mV) is larger than that of the second reduction wave (70 mV), because the charge-transfer interaction with the macrocycle becomes weaker after the first reduction of the bipyridinium unit. On the basis of the results obtained for compounds **7a−c** and the behavior of the macrocycle BPP34C10, several oxidation processes are expected. The first wave observed can be assigned to the oxidation of the macrocycle; this process occurs at more positive potential compared with the free macrocycle, because, in the rotaxane, it is involved in the above-mentioned donor−acceptor interaction. The following waves, which must involve the oxidation of the stoppers and the second oxidation of the macrocycle, are difficult to assign because of their irreversibility. For the [3]rotaxane **11a**, where two bipyridinium units are engaged in CT interactions with two macrocycles, two two-

electron reduction waves are observed at more negative potentials compared with its dumbbell-shaped component **9a**. The first wave is displaced by 110 mV, and the second one by 70 mV. This behavior is, therefore, analogous to that demonstrated by the [2]rotaxane **8a** and its dumbbell-shaped compound **7a**, except for the number of electrons involved in each process. On oxidation, several irreversible processes are observed, the first one of which can be attributed to the macrocycles, *e.g.*, as in the case of the [2]rotaxane **8a**. The [2]rotaxane **10a** shows a very interesting behavior on reduction (Table 8): four distinct, monoelectronic, and fully-reversible waves are observed. Such waves can be assigned unequivocally by comparison with the behavior of the dumbbell-shaped compound **9a** and the [3]-rotaxane **11a**. The first reduction process occurs at the same potential as the first reduction of **9a**, indicating that it relates to the bipyridinium unit not surrounded by the macrocyclic polyether. The second reduction process takes place at a potential which coincides with the first reduction process of **11a**, as expected for the first reduction of a bipyridinium unit involved in CT interaction with the macrocycle. The third and fourth reduction processes can once again be assigned to the second reduction of a free and an occupied bipyridinium unit, respectively. The oxidation behavior is analogous to that of [2]rotaxanes **8a**−**c**.

Conclusions. The π-electron rich macrocyclic polyether BPP34C10 binds bipyridinium-based guests with pseudorotaxane-like geometries, both in solution and in the solid state. These results provided the inspiration for the development of two novel synthetic approaches—namely, threading and slipping—for the self-assembly of rotaxanes composed of π-electron deficient bipyridinium-based dumbbell-shaped components and the π-electron rich hydroquinone-based macrocyclic polyether BPP34C10. The self-assembly of these molecular structures—the rotaxanes—and supramolecular complexes—the pseudorotaxanes—is driven mainly by (i) π−π stacking interactions between the bipyridinium units, incorporated within the dumbbell-shaped component, and the hydroquinone rings in BPP34C10 as well as by (ii) hydrogen bonding interactions between the acidic protons in the α-position with respect to the nitrogen atoms in the bipyridinium units and the polyether oxygen atoms of the macrocycle. By employing these synthetic methodologies, a series of [2]-, [3]-, and [4]-rotaxanes, incorporating from one to three bipyridinium recognition sites within the dumbbell-shaped component, have been self-assembled in good yields and characterized unequivocally by means of fast atom bombardment and electrospray mass spectrometries, ^{1}H NMR and ^{13}C NMR spectroscopies, and X-ray crystallography. Thus, self-assembly processes can be employed, in addition to conventional synthetic methodologies, to generate efficiently complex molecular assemblies at the nanoscopic level possessing engineered forms. The relative simplicity, the high efficiency, and the high degree of control of the threading and slipping processes suggest strongly the possibility of employing self-assembly approaches such as these to the generation of oligorotaxanes and polyrotaxanes. Furthermore, some of the self-assembled rotaxanes feature machine-like[24] properties behaving like molecular shuttles. The BPP34C10 macrocyclic component can be observed to move rapidly, on the ^{1}H NMR time scale at ambient temperature, from one bipyridinium recognition site to the other, giving rise to the so-called shuttling process. Variable temperature ^{1}H NMR spectroscopy provides the possibility of investigating, in some detail, such dynamic processes, allowing the determinination of both the rate constants and the energies of activation. The rotaxanes and their dumbbell-shaped and macrocyclic components are composed of several chromophoric and electroactive units and therefore show very interesting spectroscopic, excited state, and redox properties. Charge-transfer and energy-transfer processes involving different units have been investigated by absorption spectroscopy, luminescence spectroscopy, and excited state lifetimes. Correlations among the redox potentials of the various compounds has allowed the assignment of the reduction and oxidation processes to specific electroactive components. Ultimately, by introducing appropriate electrochemically- and/or photochemically-active subunits within the rotaxane architecture, reversible control upon the shuttling process, associated with such molecules, will be achieved by means of external stimuli. Thus, we believe that, in the near future, a new generation of "intelligent" molecular assemblies and supramolecular arrays at the nanoscopic[25] level will be generated by means of self-assembly methodologies capable of introducing function as well as controlling form. The rotaxanes described in this paper represent important steps in the progress we are making in our research laboratories toward these goals.

Experimental Section

General Methods. Chemicals were purchased from Aldrich and used as received, with the exception of 4-ethylbenzoic acid, which was purchased from Lancaster. Solvents were dried [THF (from Na/benzophenone ketyl), MeCN (from P_2O_5)] according to literature procedures. Bis-(4-*tert*-butylphenyl)phenylmethanol (**1a**)[26] as well as bis-*p*-phenylene-34-crown-10 (BPP34C10),[20] bis[4-(4-pyridyl)pyridinium]-*p*-xylylene bis(hexafluorophosphate) ([BPYPYXY][PF$_6$]$_2$),[20] and 1,1′-bis(2-hydroxyethyl)-4,4′-pyridinium bis(hexafluorophosphate) ([BHE-BIPY][PF$_6$]$_2$)[27] were prepared according to published procedures. Reactions requiring ultrahigh pressure were carried out in Teflon vessels using a custom-built ultra high pressure reactor manufactured by PSIKA Pressure Systems Limited of Glossop, UK. Thin layer chromatography (TLC) and preparative layer chromatography (PLC) were carried out on aluminium sheets coated with silica-gel 60 (Merck 5554) and glass pre-coated PLC plates with silica gel 60 (Merck 5717), respectively. Column chromatography was performed on silica-gel 60 (Merck 9385, 230−400 mesh). Melting points were determined on an Electrothermal 9200 melting point apparatus and are uncorrected. Microanalyses were performed by the University of Birmingham Microanalytical Service. Electron impact mass spectra (EIMS) were obtained from a Kratos Profile mass spectrometer. Fast atom bombardment mass spectrometry (FABMS), using a krypton primary atom beam in conjunction with a 3-nitrobenzyl alcohol or 2-nitrophenyloctyl ether matrix, was performed on a Kratos MS80RF instrument. Electrospray mass spectra (ESMS) were measured on a VG AutoSpecQ (VG Analytical Limited, Altrincham, UK). UV−visible spectra were measured and reaction kinetics followed by means of a computer-controlled Perkin-Elmer Lambda 2 spectrophotometer fitted with a thermostatic temperature controller (±0.2 °C). ^{1}H NMR spectra were recorded on Bruker AC300 (300 MHz) or AMX400 (400 MHz) spectrometers. ^{13}C NMR spectra were recorded on Bruker AC300 (75 MHz) or AMX400 (100 MHz) spectrometers.

1,1′-Bis[2-(2-hydroxyethoxy)ethyl]-4,4′-bipyridinium Bishexafluorophosphate ([BHEEBIPY][PF$_6$]$_2$). 4,4′-Bipyridine (2 g, 16.1 mmol) was dissolved in 2-methoxyethanol (100 mL), and the solution

(22) Mann, C. K.; Barnes, K. K. *Electrochemical Reactions in Non-aqueous Systems*; Dekker: New York, 1970.

(23) Balzani, V.; Scandola, F. *Supramolecular Photochemistry*; Horwood: Chichester, 1991; Chapter 5.

(24) (a) Stoddart, J. F. *Chem. Br.* **1991**, *27*, 714−718. (b) Preece, J. A.; Stoddart, J. F. In *Molecular Engineering for Advanced Materials*; Becher, J., Ed.; Kluwer: Dordrecht, 1995; pp 1−28.

(25) (a) Merkle, R. C. *Nanotechnology* **1993**, *4*, 86−90. (g) Ozin, G. A. *Adv. Mater.* **1992**, *4*, 612−649. (b) Tomalia, D. A.; Durst, H. D. *Top. Curr. Chem.* **1993**, *165*, 193−313. (c) Drexler, K. E. *Annu. Rev. Biophys. Biomol. Struct.* **1994**, *23*, 377−405.

(26) (a) Evans, A. G.; Price, A.; Thomas, J. H. *Trans. Faraday Soc.* **1954**, *50*, 16−23. (b) Gibson, H. W.; Lee, S. H.; Engen, P. T.; Lecavalier, P.; Sze, J.; Shen, Y. X.; Bheda, M. *J. Org. Chem.* **1993**, *58*, 3748−3756.

(27) Shen, Y. X.; Engen, P. T.; Berg, M. A. G.; Merola, J. S.; Gibson, H. W. *Macromolecules* **1992**, *25*, 2786−2788.

was heated to reflux under nitrogen. 2-(2-Chloroethoxy)ethanol (5 g, 40.2 mmol) in 2-methoxyethanol (25 mL) was added dropwise to this solution during 3 h. The reaction mixture was then heated under reflux for 48 h, and the solvent was removed in vacuo to yield a white solid which was recrystallized from H_2O–Me_2CO to yield [BHEEBIPY]-[PF_6]$_2$ as a white solid (3.28 g, 41%): mp 167 °C (dec), FABMS 479 $(M - PF_6)^+$; ^1H NMR (CD_3COCD_3) δ 3.61 (8H, s), 3.73 (2H, br s), 4.16 (4H, t), 5.13 (4H, t), 8.83 (4H, d), 9.43 (4H, d).

General Procedure for the Preparation of 4-Alkylphenyl-bis(4-*tert*-butylphenyl)carbinols (1b–d). The methyl esters of the 4-alkyl-benzoic acid (100 mmol) in dry THF (100 mL) were added slowly to freshly prepared THF solutions of 4-*tert*-butylphenylmagnesium bromide (5.8 g magnesium turnings, 239 mmol; 50 g of 4-*tert*-butylphe-nylbromide, 235 mmol; 100 mL of dry THF). The reaction mixtures were heated under reflux for 1 h and, after cooling, poured into the 300 g of ice containing 16 mL of concentrated H_2SO_4. After extraction with $CHCl_3$ (3 × 100 mL), the organic phases were washed with 5% aqueous solution of $NaHCO_3$ (100 mL) and H_2O (100 mL). After drying ($MgSO_4$) and evaporation of the solvent, the crude products were recrystallized from hexane. **1b** (28.9 g, 77%): mp 157–158 °C; EIMS 386 (M^+); ^1H NMR ($CDCl_3$) δ 7.31 (4H, d, $J = 8.5$ Hz), 7.18 (6H, d, $J = 8.5$ Hz), 7.11 (2H, d, $J = 8.5$ Hz), 2.71 (1H, s), 2.34 (3H, s), 1.27 (18H, s). Anal. ($C_{28}H_{34}O$) C, H. **1c** (30.6 g, 76%): mp 118–119 °C; EIMS 399 (M - 1)$^+$ ^1H NMR ($CDCl_3$) δ 7.31 (4H, d, $J = 8.5$ Hz), 7.11–7.22 (8H, m), 2.73 (1H, s), 2.64 (2H, q, $J = 7.5$ Hz) 1.31 (18H, s), 1.23 (3H, t, $J = 7.5$ Hz). Anal. ($C_{29}H_{36}O$) C,H. **1d** (30.4 g, 73%): mp 156–158 °C, EIMS 413 (M - 1)$^+$, ^1H NMR ($CDCl_3$) δ 7.32 (4H, d, $J = 8.5$ Hz), 7.13–7.22 (8H, m), 2.90 (1H, septet, $J = 7$ Hz), 2.74 (1H, s), 1.31 (18H, s), 1.24 (6H, d, $J = 7$ Hz). Anal. ($C_{30}H_{38}O$) C, H.

Tris(4-*tert*-butylphenyl)methanol (1e).[27,28] 1-Bromo-4-*tert*-butyl-benzene (6.1 g, 28.6 mmol) was dissolved in dry THF (45 mL), and the solution was stirred at 0 °C under argon. Magnesium turnings (0.72 g, 30.0 mmol), pretreated with iodine vapor, were added to the solution under argon, and stirring was continued at 0 °C until the reaction was observed to initiate. The reaction mixture was then warmed up slowly to room temperature over 30 min and held at this temperature until the reaction subsided. Diethyl carbonate (1.35 g, 11.4 mmol) was added dropwise to the solution of Grignard reagent in dry THF (20 mL). The reaction mixture was stirred at room temperature for 2 h. The solvent was then removed in vacuo, and the residue washed with ice-cooled pentane to remove unreacted 1-bromo-4-*tert*-butylbenzene. The result-ing solid was recrystallized from light petroleum (bp 60–80 °C) to yield the product, tris(4-*tert*-butylphenyl)methanol as a colorless solid (3.34 g, 77%) mp 213–214 °C (lit.[27] 215–216 °C, lit.[28] 212–213 °C), EIMS 411 (M - OH)$^+$, ^1H NMR ($CDCl_3$), δ 1.35 (27H, s), 2.82 (1H, br s), 7.27 (6H, d, $J = 9$ Hz), 7.39 (6H, d, $J = 9$ Hz).

General Procedure for the Preparation of 4-Alkylphenyl-bis(4-*tert*-butylphenyl)methyl Chlorides (2a–e). The substituted carbinols (1a–e, 40 mmol) were dissolved in dry benzene (25 mL), and freshly distilled acetyl chloride (7 mL) was added. The reaction mixtures were heated under reflux for 30 min. After allowing the reaction mixtures to cool down to room temperature, hexane (120 mL) was added, and the mixtures were left at 5 °C overnight. White crystals of the chlorides were filtered off quickly. After drying, they were used immediately in the next step. **2a** (12.6 g, 80%): mp 161–164 °C; EIMS 356 (M - Cl)$^+$; ^1H NMR ($CDCl_3$) δ 7.28 (4H, d, $J = 8.5$ Hz), 7.08–7.21 (9H, m), 1.31 (18H, m). **2b** (13.7 g, 87%): mp 192–194 °C; EIMS 369 (M - Cl)$^+$; ^1H NMR ($CDCl_3$) δ 7.30 (4H, d, $J = 8.5$ Hz), 7.07–7.20 (8H, m), 2.35 (3H, s), 1.32 (18H, s). **2c** (14.3 g, 85%): mp 183–185 °C; EIMS 383 (M - Cl)$^+$; ^1H NMR ($CDCl_3$) δ 7.30 (4H, d, $J = 8.5$ Hz), 7.10–7.21 (8H, m), 2.66 (2H, q, $J = 7.5$ Hz), 1.32 (18H, s), 1.25 (3H, t, $J = 7.5$ Hz). **2d** (15.1 g, 87%): mp 198–199 °C; EIMS 397 (M - Cl)$^+$; ^1H NMR ($CDCl_3$) δ 7.31 (6H, d, $J = 8.5$ Hz), 7.07–7.21 (8H, m), 2.88 (1H, septet, $J = 6.5$ Hz), 1.31 (18H, s), 1.25 (6H, d, $J = 6.5$ Hz). **2e** (14.3 g, 80%): mp 211–213 °C; FABMS 446 (M^+); ^1H NMR ($CDCl_3$) δ 7.27 (6H, d, $J = 9$ Hz), 7.10 (6H, d, $J = 9$ Hz), 1.30 (27H, s).

General Procedure for the Preparation of 4-[4-Alkylphenylbis-(4-*tert*-butylphenyl)methyl]phenols (3a–e). Freshly prepared trityl

chlorides (**2a–e**, 35 mmol) were added portionwise to molten phenol (25 g), and the reaction mixtures were heated at 110 °C overnight. The resulting white solids were treated with 40% aqueous KOH (140 g), washed thoroughly with H_2O, and dried. The resulting potassium salts were used in the next step without further purification. Small samples of the phenolates were treated with dilute acetic acid, and the crude phenols were recrystallized from hexane. **3a** (16.6 g, 97%): mp 227–228 °C; FABMS 448 (M^+); ^1H NMR ($CDCl_3$) δ 7.16–7.28 (9H, m) 7.02–7.12 (6H, m), 6.70 (2H, d, $J = 9$ Hz), 1.60 (1H, br s), 1.30 (18H, s). Anal. ($C_{33}H_{36}O$) C, H. **3b** (16.7 g, 95%): mp 163–165 °C; FABMS 462 (M^+); ^1H NMR ($CDCl_3$) δ 6.88–7.19 (14H, m), 6.48 (2H, d, $J = 8.5$ Hz), 4.69 (1H, br s), 2.23 (3H, s), 1.24 (18H, s). Anal. ($C_{34}H_{38}O$) C, H. **3c** (17.5 g, 97%): mp 208–209 °C; FABMS 476 (M^+); ^1H NMR ($CDCl_3$) δ 7.23 (4H, d, $J = 8.5$ Hz), 7.02–7.12 (10H, m), 6.70 (2H, d, $J = 8.5$ Hz), 4.73 (1H, br s), 2.63 (2H, q, $J = 7$ Hz), 1.30 (18H, s), 1.23 (3H, t, $J = 7.5$ Hz). Anal. ($C_{35}H_{40}O$) C, H. **3d** (18.1 g, 98%): mp 214–216 °C; FABMS 490 (M^+); ^1H NMR ($CDCl_3$) δ 7.23 (4H, d, $J = 8.5$ Hz), 7.01–7.12 (10H, m), 6.69 (2H, d, $J = 8.5$ Hz), 4.99 (1H, br s), 2.87 (1H, septet, $J = 6.5$ Hz), 1,29 (18H, s), 1.23 (6H, d, $J = 6.5$ Hz). Anal. ($C_{36}H_{42}O$) C, H. **3e** (18.1 g, 95%): mp 304–306 °C; FABMS 504 (M^+); ^1H NMR ($CDCl_3$) d 7.27 (6H, d, $J = 9$ Hz), 7.05–7.10 (8H, m), 6.69 (2H, d, $J = 8$ Hz), 1.30 (27H, s). Anal. ($C_{38}H_{44}O$).C, H. The yields, which are quoted, are for the potassium phenolates.

General Procedure for the Preparation of 2-[2-[4-Alkylphenyl-bis(4-*tert*-butylphenyl)methoxy]ethoxy]ethanols (4a–e). The potas-sium salts of the substituted trityl phenols (**3a–e**, 30 mmol) were added to a mixture of dry MeCN (100 mL), K_2CO_3 (2 g, 15 mmol), and 2-(chloroethoxy)ethanol (7.5 g, 60 mmol). The reaction mixtures were heated under reflux for 5 days. After cooling them down to room temperature, the reaction mixtures were filtered through Celite before the solvent was removed. The crude products were recrystallized from hexane. **4a** (14.2 g, 88%): mp 141–142 °C; FABMS 536 (M^+); ^1H NMR ($CDCl_3$) δ 7.16–7.34 (9H, m), 7.06–7.14 (6H, m), 6.79 (2H, d, $J = 9$ Hz), 4.08–4.15 (2H, m), 3.82–3.90 (2H, m), 3.72–3.80 (2H, m) 3.64–3.72 (2H, m), 1.63 (1H, br s), 1.30 (18H, s). Anal. ($C_{37}H_{44}O_3$) C, H. **4b** (13,7 g, 83%): mp 145–146 °C; FABMS 550 (M^+); ^1H NMR ($CDCl_3$) δ 7.23 (4H, d, $J = 8.5$ Hz), 7.01–7.13 (10H, m), 6.78 (2H, d, $J = 8.5$ Hz), 4.08–4.15 (2H, m), 3.83–3.90 (2H, m), 3.73–3.80 (2H, m), 3.65–3.70 (2H, m), 2.32 (3H, s), 2.21 (1H, br s), 1.30 (18H, s). Anal. ($C_{38}H_{46}O_3$) C, H. **4c** (15.1 g, 89%): mp 97–99 °C; FABMS 564 (M^+); ^1H NMR ($CDCl_3$) δ 7.23 (4H, d, $J = 8.5$ Hz), 7.03–7.13 (10H, m), 6,79 (2H, d, $J = 8.5$ Hz), 4.09–4.14 (2H, m), 3.83–3.89 (2H, m), 3.73–3.81 (2H, m), 3.64–3.70 (2H, m), 2.62 (2H, q, $J = 7.5$ Hz), 2.23 (1H, br s), 1.30 (18H, s), 1.23 (3H, t, $J = 7.5$ Hz). Anal. ($C_{39}H_{48}O_3$) C, H. **4d** (13.0 g, 75%): mp 158–160 °C; FABMS 578 (M^+); ^1H NMR ($CDCl_3$) δ 7.23 (4H, d, $J = 8.5$ Hz), 7.05–7.12 (10H, m), 6.78 (2H, d, $J = 8.5$ Hz), 4.09–4.14 (2H, m), 3.83–3.89 (2H, m), 3.73–3.80 (2H, m), 3.61–3.70 (2H, m), 2.87 (1H, septet, $J = 6.5$), 2.18 (1H, br s), 1.30 (18H, s), 1.24 (6H, d, $J = 6.5$ Hz). Anal. ($C_{40}H_{50}O_3$) C, H. **4e** (16.4 g, 92%): mp 280–282 °C; FABMS 592 (M^+); ^1H NMR ($CDCl_3$) δ 7.23 (6H, d, $J = 8.5$ Hz), 7.05–7.10 (8H, m), 6.78 (2H, d, $J = 8.5$ Hz), 4.09–4.14 (2H, m), 3.82–3.85 (2H, m), 3.74–3.78 (2H, m), 3.65–3.69 (2H, m), 2.41 (1H, br s), 1.30 (27H, s). Anal. ($C_{41}H_{52}O_3$) C, H.

General Procedure for the Preparation of the Tosylates (5a–c) of the 2-[2-[4-Alkylphenylbis(4-*tert*-butylphenyl)methoxy]ethoxy]-ethanols. Solid tosyl chloride (6.5 g, 34 mmol) was added in several portions with vigorous stirring to the ice-cooled mixtures of alcohols (**4a–e**, 30 mmol), partitioned between 30% aqueous NaOH (25 g) and benzyltriethylammonium bromide (0.3 g, 1.1 mmol) in CH_2Cl_2 (60 mL). The reaction mixtures were allowed to warm up to room temperature before being stirred overnight. H_2O (50 mL) was added, and the mixtures were extracted with CH_2Cl_2 (3 × 50 mL). The organic phases were washed with H_2O and dried ($MgSO_4$). After evaporation of the solvent, the crude products were recrystallized from EtOH. **5a** (12.0 g, 58%): mp 115–116 °C; FABMS 690 (M^+); ^1H NMR ($CDCl_3$) δ 7.79 (2H, d, $J = 8$ Hz), 7.16–7.32 (11H, m), 7.04–7.16 (6H, m), 6.75 (2H, d, $J = 9$ Hz), 4.15–4.23 (2H, m), 3.96–4.05 (2H, m), 3.70–3.81 (4H, m), 2.38 (3H, s), 1.30 (18H, s). Anal. ($C_{44}H_{50}O_5S$) C, H. **5b** (12.7 g, 60%): mp 72–73 °C; FABMS 704 (M^+); ^1H NMR ($CDCl_3$) δ 7.79 (2H, d, $J = 8$ Hz), 7.19–7.30 (4H, m), 7.04–7.13 (12H, m),

(28) Marvel, C. S; Kaplan, J. F.; Himel, C. M. *J. Am. Chem. Soc.* **1941**, *63*, 1892–1896.

6.75 (2H, d, *J* = 9 Hz), 4.15–4.22 (2H, m), 3.97–4.03 (2H, m), 3.72–3.80 (4H, m), 2.31 (3H, s), 2.38 (3H, s), 1.30 (18H, s). Anal. (C₄₅H₅₂O₅S) C, H. **5c** (12.1 g, 56%): mp 93–95 °C; FABMS 718 (M⁺); ¹H NMR (CDCl₃) δ 7.79 (2H, *J* = 8 Hz), 7.20–7.31 (4H, m), 7.03–7.13 (12H, m), 6.74 (2H, d, *J* = 9 Hz), 4.16–4.22 (2H, m), 3.98–4.03 (2H, m), 3.72–3.79 (4H, m), 2.63 (2H, q, *J* = 7.5 Hz), 3.39 (3H, s), 1.30 (18H, s), 1.23 (3H, t, *J* = 7.5 Hz). Anal. (C₄₆H₅₄O₅S) C, H. **5d** (17.1 g, 78%): mp 124–126 °C; FABMS 732 (M⁺); ¹H NMR (CDCl₃) δ 7.79 (2H, d, *J* = 8 Hz), 7.20–7.30 (4H, m), 7.04–7.13 (12H, m), 6.74 (2H, d, *J* = 9 Hz), 4.16–4.22 (2H, m), 3.98–4.04 (2H, m), 3.72–3.80 (4H, m), 2.87 (1 H, septet, *J* = 7 Hz), 2.38 (3H, s), 1.30 (18H, s), 1.24 (6H, d, *J* = 7 Hz). Anal. (C₅₀H₆₀O₅S) C, H. **5e** (17.5 g, 78%): mp 197–199 °C; FABMS 746 (M⁺); ¹H NMR (CDCl₃) δ 7.79 (2H, d, *J* = 8 Hz), 7.20–7.30 (8H, m), 7.06–7.11 (8H, m), 6.74 (2H, d, *J* = 8 Hz), 4.17–4.21 (2H, m), 3.99–4.03 (2H, m), 3.90–3.96 (4H, m), 2.38 (3H, s), 1.30 (27H, s). Anal. (C₄₈H₅₈O₅S) C, H.

General Procedure for the Preparation of the 4-[2-[2-[4-Alkyl-phenyl-bis(4-*tert*-butylphenyl)methoxy]ethoxy]ethoxybenzylic Alcohols (6a–e). K₂CO₃ (5 g, 36 mmol) was suspended in dry MeCN (100 mL) under nitrogen, and 4-hydroxybenzyl alcohol (2.5 g, 20 mmol) was added during 10 min. The suspension was stirred under reflux for 30 min. The tosylates (**5a–e**, 18 mmol) were added and the reaction mixtures were stirred under reflux for 48 h. After cooling and filtration through Celite, solvent was evaporated, and the crude products were recrystallized from PhMe/hexane. **6a** (9.3 g, 80%): mp 118–120 °C; FABMS 642 (M⁺); ¹H NMR (CDCl₃) δ 7.16–7.32 (11H, m), 7.04–7.14 (6H, m), 6.90 (2H, d, *J* = 8.5 Hz), 6.79 (2H, d, *J* = 9 Hz), 4.62 (2H, s), 4.09–4.20 (4H, m), 3.88–3.98 (4H, m), 1.30 (18H, s). Anal. (C₄₄H₅₀O₄) C, H. **6b** (9.6 g, 81%): mp 102–104 °C; FABMS 656 (M⁺); ¹H NMR (CDCl₃) δ 7.19–7.30 (6H, m), 7.01–7.11 (10H, m), 6.91 (2 H, d, *J* = 8.5 Hz), 6.78 (2H, d, *J* = 8.5 Hz), 4.61 (2H, s), 4.10–4.18 (4H, m), 3.89–3.95 (4H, m), 2.31 (3H, s), 1.30 (18H, s). Anal. (C₄₅H₅₂O₄) C, H. **6c** (10.3 g, 85%): mp 107–109 °C; FABMS 670 (M⁺); ¹H NMR (CDCl₃) δ 7.15–7.29 (6H, m), 7.02–7.12 (10H, m), 6.90 (2H, d, *J* = 8.5 Hz), 6.78 (2H, d, *J* = 9 Hz), 4.60 (2H, s), 4.09–4.17 (4H, m), 3.88–3.95 (4H, m), 2.62 (2H, q, *J* = 6.5 Hz), 1.29 (18H, s), 1.23 (3H, t, *J* = 6.5 Hz). Anal. (C₄₆H₅₄O₄) C, H. **6d** (9.1 g, 74%): mp 121–123 °C; FABMS 684 (M⁺); ¹H NMR (CDCl₃) δ 7.20–7.29 (6H, m), 7.04–7.12 (10H, m), 6.90 (2H, d, *J* = 8.5 Hz), 6.78 (2H, d, *J* = 9 Hz), 4.60 (2H, s), 4.09–4.17 (4H, m), 3.88–3.96 (4H, m), 2.87 (1H, septet, *J* = 7 Hz), 1.30 (18H, s), 1.24 (6H, d, *J* = 7 Hz). Anal. (C₄₇H₅₆O₄) C, H. **6e** (11.4 g, 91%): mp 292–294 °C; FABMS 698 (M⁺); ¹H NMR (CDCl₃) δ 7.28 (2H, d, *J* = 8 Hz), 7.23 (6H, d, *J* = 9 Hz) 7.06–7.11 (8H, m), 6.91 (2H, d, *J* = 8 Hz) 6.79 (2H, d, *J* = 8.Hz), 4.61 (2H, s), 4.11–4.18 (4H, m), 3.89–3.95 (4H, m), 1.30 (27 H, s). Anal. (C₄₈H₅₈O₄) C, H.

General Procedure for the Preparation of the *N*,*N*′-Bis[4-[2-[2-[4-Alkylphenylbis(4-*tert*-butylphenyl)methoxy]ethoxy]ethoxybenzyl]-4,4′-bipyridinium Bis(hexafluorophosphate) (7a–e). The substituted benzyl alcohols (**6a–e**, 3 mmol) were dissolved in dry THF (15 mL), and *N*-chlorosuccinimide (0.44 g, 3.3 mmol) and Ph₃P (0.87 g, 3.3 mmol) were added under vigorous stirring during 30 min. The reaction mixtures were stirred under nitrogen at room temperature for 15 h and then quickly subjected to chromatography on short columns [SiO₂, hexane–EtOAc (4:1)]. Solvent was evaporated off and the glassy solids were dissolved in dry MeCN (20 mL). 4,4′-Bipyridine (101 mg, 0.65 mmol) was added, and the reaction mixtures were stirred and heated at reflux under nitrogen for 2 days. After cooling down to room temperature, the yellowish solids were filtered off and washed with small amounts of MeCN. The residues were then dissolved in a H₂O–Me₂CO mixture, and saturated aqueous NH₄PF₆ (20 mL) was added. The Me₂CO was evaporated off under reduced pressure, and the yellowish solids were filtered off and washed with H₂O. The crude products were subjected to chromatography [SiO₂, MeOH–CH₂Cl₂–MeNO₂–2 M NH₄Cl (70:16:11:3)], and the purified components were dissolved in H₂O–Me₂CO mixtures. Saturated aqueous NH₄PF₆ was added, and the Me₂CO was evaporated off, leaving yellowish solids, which were filtered off and washed with H₂O, before drying. **7a** (254 mg, 23%): mp 226–228 °C (dec); FABMS 1408 (M - 2PF₆)⁺; ¹H NMR (CD₃COCD₃) δ 9.50 (4H, d, *J* = 7 Hz), 8.83 (4H, d, *J* = 7 Hz), 7.62 (4H, d, *J* = 8.5 Hz), 7.04–7.34 (34H, m), 6.85 (4H, d, *J* = 9 Hz), 6.10 (4H, s), 4.17–4.22 (4H, m), 4.11–4.16 (4H, m), 3.86–3.92

(8H, m), 1.29 (36H, s); ¹³C NMR (CD₃CN) δ 161.3, 157.8, 149.6, 148.6, 148.3, 145.4, 140.6, 132.8, 132.3, 131.6, 131.3, 128.6, 126.8, 125.5, 125.3, 116.5, 114.4, 70.5, 70.3, 68.8, 68.4, 65.4, 64.4, 35.0, 31.6. Anal. (C₉₈H₁₀₆N₂O₆P₂F₁₂) C, H, N. **7b** (426 mg, 38%): mp 213–215 °C (dec); FABMS 1436 (M - 2PF₆)⁺; ¹H NMR (CD₃COCD₃) δ 9.48 (4H, d, *J* = 7 Hz), 8.81 (4H, d, *J* = 7 Hz), 7.65 (4H, d, *J* = 8.5 Hz), 7.32 (8H, d, *J* = 8.5 Hz), 7.06–7.16 (24H, m) 6.86 (4H, d, *J* = 9 Hz), 6.11 (4H, s), 4.18–4.24 (4H, m), 4.12–4.18 (4H, m), 3.87–3.95 (8H, m), 2.30 (6H, s), 1.31 (36H, s); ¹³C NMR (CD₃CN) δ 161.3, 157.7, 151.1, 149.5, 146.3, 145.6, 145.5, 140.7, 136.4, 132.8, 132.3, 131.5, 131.3, 129.2, 128.3, 125.5, 125.3, 116.5, 114.4, 70.5, 70.3, 68.8, 68.4, 65.4, 64.1, 35.0, 31.6, 20.9. Anal. (C₁₀₀H₁₁₀N₂O₆P₂F₁₂) C, H, N. **7c** (558 mg, 49%), mp 218–220 °C (dec); FABMS 1464 (M - 2PF₆)⁺; ¹H NMR (CD₃COCD₃), δ 9.45 (4H, d, *J* = 7 Hz), 8.78 (4H, d, *J* = 7Hz), 7.63 (4H, d, *J* = 8.5), 7.30 (8H, d, 8.5 Hz), 7.04–7.15 (24H, m) 6.84 (4H, d, *J* = 9 Hz), 6.08 (4H, s), 4.16–4.22 (4H, m), 4.10–4.16 (4H, m) 3.85–3.92 (8H, m), 2.60 (4H, q, *J* = 7.5 Hz), 1.29 (36H, s), 1.20 (6H, t, *J* = 7.5 Hz); ¹³C NMR (CD₃CN) δ 161.3, 157.7, 151.4, 149.5, 146.3, 145.8, 145.6, 142.7, 140.8, 132.8, 132.3, 131.6, 131.3, 128.3, 128.0, 125.5, 125.3, 116.5, 114.4, 70.5, 70.3, 68.8, 68.4, 65.4, 64.1, 35.0, 31.6, 28.9, 15.9. Anal. (C₁₀₂H₁₁₄N₂O₆P₂F₁₂) C, H, N. **7d** (530 mg, 44%): mp 209–211 °C (dec); FABMS 1492 (M - 2PF₆)⁺; ¹H NMR (CD₃-COCD₃) δ 9.46 (4H, d, *J* = 7 Hz), 8.78 (4H, d, *J* = 7Hz), 7.63 (4H, d, *J* = 8.5 Hz), 7.30 (8H, d, *J* = 8.5 Hz), 7.05–7.17 (24H, m), 6.84 (4H, d, *J* = 9 Hz), 6.08 (4H, s), 4.17- 4.22 (4H, m), 4.10–4.17 (4H, m), 3.85–3.92 (8H, m), 2.86 (2H, septet, *J* = 7 Hz), 1.29 (36H, s), 1.22 (12H, d, *J* = 7 Hz); ¹³C NMR (CD₃CN) δ 161.3, 157.7, 151.1, 149.5, 146.3, 145.6, 145.5, 141.7, 138.3, 132.6, 132.3, 131.5, 131.3, 129.2, 128.3, 126.5, 125.5, 116.5, 114.4, 70.5, 70.3, 68.8, 68.4, 65.4, 64.1, 35.0, 34.2, 31.6, 24.2. Anal. (C₁₀₄H₁₁₈N₂O₆P₂F₁₂) C, H, N. **7e** (787 mg, 67%): mp 200 °C (dec); FABMS 1518 (M - 2PF₆)⁺; ¹H NMR (CD₃COCD₃) δ 9.36 (4H, d, *J* = 7 Hz), 8.50 (4H, d, *J* = 7 Hz), 7.70 (4H, d, *J* = 8.5), 7.23 (12H, d, *J* = 8.5 Hz), 7.05–7.10 (16H, m), 6.89 (4H, d, *J* = 8.5 Hz), 6.78 (4H, d, *J* = 9 Hz), 6.07 (4H, s), 4.11–4.18 (8H, m), 3.90–3.96 (8H, m), 1.30 (54H, s). Anal. (C₁₀₆H₁₂₂N₂O₆P₂F₁₂) C, H, N.

General Procedure for the Preparation of the [2]Rotaxanes 8a–c. The bipyridinum salts (**7a–c**, 0.07 mmol) were dissolved in MeCN (7 mL), and BPP34C10 (150 mg, 0.28 mmol) was added. The reaction mixtures were stirred at 55 °C for 10 days. MeCN was evaporated off, and Me₂CO (3 mL) added. The white crystals of BPP34C10 were filtered off and washed with small amounts of Me₂CO. The red Me₂-CO solutions were concentrated at room temperature and purified by PLC [SiO₂, MeOH–MeNO₂–CH₂Cl₂ (6:1:1)] which afforded the stable [2]rotaxanes as deep orange solids. **8a** (81 mg, 52%): mp 146–149 °C (dec); FABMS 1944 (M - 2PF₆)⁺; ¹H NMR (CD₃COCD₃) δ 9.19 (4H, d, *J* = 7 Hz), 8.27 (4H, d, *J* = 7 Hz), 7.74 (4H, d, *J* = 9 Hz), 7.05–7.34 (34H, m), 6.83 (4H, d, *J* = 9 Hz), 6.10 (8H, s), 6.04 (4H, s), 4.18–4.25 (4H, m), 4.09–4.16 (4H, m), 3.85–3.93 (8H, m), 3.78 (16H, br s), 3.72–3.77 (8H, m), 3.62–3.67 (8H, m), 1.29 (36H, s); ¹³C NMR (CD₃CN) δ 161.1, 157.7, 153.0, 149.6, 148.5, 147.2, 146.3, 145.3, 140.5, 132.8, 132.7, 131.6, 131.3, 128.5, 126.8, 126.4, 125.5, 116.3, 116.2, 115.7, 114.4, 71.4, 71.2, 70.7, 70.5, 70.3, 68.8, 68.5, 68.4, 64.9, 64.4, 34.9, 31.6. Anal. (C₁₂₆H₁₄₆N₂O₁₆P₂F₁₂) C, H, N. **8b** (71 mg, 45%): mp 137–140 °C (dec); FABMS 1972 (M-2PF₆)⁺; ¹H NMR (CD₃COCD₃) δ 9.18 (4H, d, *J* = 7 Hz), 8.27 (4H, d, *J* = 7 Hz), 7.74 (4H, d, *J* = 9 Hz), 7.27 (8H, d, *J* = 9 Hz), 7.03–7.17 (24H, m), 6.82 (4H, d, *J* = 9 Hz), 6.10 (8H, s), 6.04 (4H, s), 4.18–4.25 (4H, m), 4.09–4.16 (4H, m), 3.85–3.93 (8H, m), 3.78 (16H, bs), 3.72–3.77 (8H, m), 3.62–3.67 (8H, m), 2.28 (6H, s), 1.28 (36H, s); ¹³C NMR (CD₃CN) δ 161.3, 157.7, 153.1, 149.6, 148.5, 147.2, 146.3, 145.6, 140.8, 132.8, 132.6, 131.5, 131.3, 129.9, 126.8, 126.2, 125.5, 117.8, 116.5, 116.2, 115.7, 114.4, 71.5, 71.3, 70.7, 70.5, 70.3, 68.9, 68.6, 68.4, 65.1, 64.5, 35.0, 31.6, 20.9. Anal. (C₁₂₈H₁₅₀N₂O₁₆P₂F₁₂) C, H, N. **8c** (75 mg, 47%): mp 140–144 °C (dec); FABMS 2000 (M - 2PF₆)⁺; ¹H NMR (CD₃COCD₃) δ 9.19 (4H, d, *J* = 7 Hz), 8.28 (4H, d, *J* = 7 Hz), 7.74 (4H, d, *J* = 9 Hz), 7.29 (8H, d, *J* = 9 Hz), 7.03–7.17 (24H, m), 6.82 (4H, d, *J* = 9 Hz), 6.10 (8H, s), 6.05 (4H, s), 4.18–4.25 (4H, m), 4.09–4.16 (4H, m), 3.85–3.93 (8H, m), 3.78 (16H, bs), 3.72–3.77 (8H, m), 3.62–3.67 (8H, m), 2.60 (4H, q, *J* = 7 Hz), 1,29 (36H, s), 1.20 (6H, t, *J* = 7 Hz); ¹³C NMR (CD₃CN) δ 161.2, 157.7, 153.1, 149.5, 147.2, 146.2, 145.8, 145.5, 142.7, 140.7, 132.7, 132.6, 131.6,

131.3, 128.0, 126.2, 126.1, 125.4, 116.4, 115.7, 114.3, 71.4, 71.2, 70.7, 70.5, 70.3, 68.8, 65.5, 68.4, 65.1, 64.1, 35.0, 31.6, 28.8, 15.9. Anal. ($C_{130}H_{154}N_2O_{16}P_2F_{12}$) C, H, N.

[2]Rotaxane 8e. Method A. 4,4′-Bipyridine (31 mg, 0.2 mmol), BPP34C10 (214 mg, 0.4 mmol), and 1-[2-(4-chloromethylphenoxy)-ethoxy]-4-[tris(4-*tert*-butylphenyl)methyl]benzene (307 mg, 0.43 mmol) were dissolved in anhydrous DMF (6 mL), and the solution was placed in a Teflon ultra high pressure reaction vessel which was subjected to a pressure of 12 kbar at 30 °C for 2 days. The reaction mixtures were poured into H_2O (60 mL), and a saturated aqueous solution of NH_4PF_6 was added. This solution was extracted with $MeNO_2$ (2 × 25 mL), and the combined organic layers were washed and dried ($MgSO_4$). Removal of the solvent under reduced pressure gave an orange solid, which was purified by column chromatography [SiO_2, Me_2CO–hexane (3:2)] to give the [2]rotaxane **8e** as a glassy orange solid (120 mg, 26%): mp 205–210 °C (dec); FABMS 2201 (M - PF_6)⁺; ¹H NMR (CD_3COCD_3) δ 9.19 (4H, d, *J* = 7 Hz), 8.28 (4H, d, *J* = 7 Hz), 7.79 (4H, d, *J* = 8.5 Hz), 7.30 (12H, d, *J* = 8.5 Hz), 7.03–7.17 (20H, m), 6.81 (4H, d, *J* = 9 Hz), 6.10 (8H, s), 6.05 (4H, s), 4.18–4.25 (4H, m), 4.09–4.16 (4H, m), 3.85–3.93 (8H, m), 3.79 (16H, s), 3.72–3.77 (8H, m), 3.62 –3.67 (8H, m), 1.29 (54H, s); ¹³C NMR (CD_3CN) δ 161.2, 157.7, 153.1, 149.5, 147.2, 146.2, 145.5, 140.7, 132.7, 132.6, 131.2, 126.2, 126.1, 125.4, 116.4, 115.7, 114.3, 71.4, 71.2, 70.7, 70.5, 70.3, 68.8, 65.5, 68.4, 65.1, 64.0, 35.0, 31.6. Anal. ($C_{134}H_{162}N_2O_{16}P_2F_{12}$) C, H, N.

Method B. 4,4′-Bipyridine (55 mg, 0.35 mmol), BPP34C10 (536 mg, 1 mmol) and 1-[2-(4-chloromethylphenoxy)ethoxy)ethoxy]-4-[tris-(4-*tert*-butylphenyl)methyl]benzene (698 mg, 0.97 mmol) were dissolved in dry MeCN (5 mL). The reaction mixture was stirred under a nitrogen atmosphere for 15 days. The solvent was removed under reduced pressure to yield an off-white solid, which was subjected to counterion exchange with a saturated aqueous NH_4PF_6 solution. This mixture contained only starting material and the bipyridinium bis-(hexafluorophosphate) **7e** (137 mg, 21%). No rotaxane could be isolated or detected.

Method C. The bipyridinium bis(hexafluorophosphate) **7e** (90 mg, 0.05 mmol) and BPP34C10 (54 mg, 0.1 mmol) were dissolved in anhydrous DMF (2.5 mL), placed in a Teflon ultrahigh pressure reaction vessel, and subjected to a pressure of 12 kbar at 30 °C for 48 h. Only starting compounds were recovered.

Bis[*N*-4-[2-[2-[phenyl-bis(4-*tert*-butylphenyl)methoxy]ethoxy]-ethoxybenzyl-4,4′-bipyridinium-*N*′-*p*-xylylene Tetrakis(hexafluorophosphate) (9a). The substituted benzyl acohol **6a** (1.29 g, 2 mmol) was chlorinated, employing the same procedure as that described for **7a**–**e** and [BPYPYXY][PF_6]₂ (0.36 g, 0.5 mmol) was added to a MeCN solution of the corresponding chloride. The reaction mixture was stirred and heated under reflux for 2 days. After cooling to room temperature, the yellowish solid was filtered off and washed with small amounts of cold MeCN before being dissolved in a H_2O–Me_2CO mixture. Saturated aqueous NH_4PF_6 was added, and Me_2CO was evaporated off under reduced pressure. The precipitate was filtered off, washed with H_2O, and subjected to column chromatography [SiO_2, MeOH–CH_2-Cl_2–$MeNO_2$–2 M NH_4Cl (6:2:1:1)]. The pure compound was dissolved in a H_2O–Me_2CO mixture. Saturated aqueous NH_4PF_6 was added, the Me_2CO was evaporated off, and the resulting lustrous yellowish solid was washed with H_2O and MeOH before being dried under vacuum (0.495 g, 44%). **9a**: mp 280–285 °C (decomp); FABMS 2103 (M - PF_6)⁺, 1958 (M - 2PF_6)⁺, 1813 (M - 3PF_6)⁺; ¹H NMR (CD_3COCD_3) δ 9.44 (4H, d, *J* = 6.5 Hz), 9.43 (4H, d, *J* = 6.5 Hz), 8.76 (4H, d, *J* = 6.5 Hz), 8.75 (4H, d, *J* = 6.5), 7.79 (4H, s), 7.63 (4H, d, *J* = 8.5 Hz), 7.04–7.34 (34H, m), 6.85 (4H, d, *J* = 9 Hz), 6.21 (4H, s), 6.08 (4H, s), 4.17–4.22 (4H, m), 4.11–4.16 (4H, m), 3.85–3.92 (8H, m), 1.29 (36H, s); ¹³C NMR (CD_3CN) δ 161.5, 157.9, 151.8, 149.8, 148.7, 146.8, 146.5, 145.6, 140.8, 135.5, 133.0, 132.5, 131.8, 131.6, 131.5, 128.7, 128.5, 127.0, 125.7, 125.5, 118.5, 116.7, 114.6, 70.7, 70.4, 68.9, 68.6, 65.6, 65.2, 64.6, 35.1, 31.8. Anal. ($C_{116}H_{122}N_4O_6P_4F_{24}$) C, H, N.

[2]Rotaxane 10a. The tetracationic dumbbell-shaped compound **9a** (112.4 mg, 0.05 mmol) was dissolved in dry MeCN (5 mL) and BPP34C10 (108 mg, 0.2 mmol) was added. After heating at 55 °C for 10 days, MeCN was evaporated off at room temperature, and Me_2-CO (3 mL) was added. Crystalline BPP34C10 was filtered off, and

the red Me_2CO solution was purified directly by PLC [SiO_2, MeOH–CH_2Cl_2–$MeNO_2$–2 M NH_4Cl (70:16:11:3)]. After evaporation of the solvents, the pure product containing NH_4Cl was dissolved in a H_2O–Me_2CO mixture, and the tetrakis(hexafluorophosphate) was precipitated by addition of saturated aqueous NH_4PF_6. The orange red solid was washed with H_2O and dried under vacuum (43 mg, 31%). **10a**: mp 140–145 °C (dec); FABMS 2639 (M - PF_6)⁺, 2494 (M - 2PF_6)⁺, 2349 (M - 3PF_6)⁺; ¹H NMR (CD_3COCD_3) δ 9.30 (4H, d, *J* = 6.5 Hz), 9.26 (4H, d, *J* = 6.5 Hz), 8.45 (4H, d, *J* = 6.5 Hz), 8.42 (4H, d, *J* = 6.5 Hz), 7.89 (4H, s), 7.66 (4H, d, *J* = 8.5 Hz), 7.05–7.32 (34H, m), 6.82 (4H, d, *J* = 9 Hz), 6.18 (4H, s), 6.05 (8H, s), 6.03 (4H, s), 4.17–4.22 (4H, m), 4.10–4.14 (4H, m), 3.85–3.90 (8H, m), 3.76 (16H, s), 3.70–3.74 (8H, m), 3.62–3.66 (8H, m), 1.28 (36H, s); ¹³C NMR (CD_3CN) δ 161.2, 157.7, 153.1, 149.6, 148.6, 146.6, 146.3, 145.4, 140.6, 135.7, 132.8, 132.5, 131.6, 131.5, 131.3, 128.6, 127.4, 127.2, 126.8, 125.5, 118.5, 118.3, 116.6, 114.4, 71.4, 71.2, 70.7, 70.5, 70.3, 68.8, 65.5, 68.4, 65.2, 64.9, 64.4, 35.0, 31.6. Anal. ($C_{144}H_{162}N_4O_{16}P_4F_{24}$) C, H, N. The [3]rotaxane **11a** (13 mg, 8%) was also isolated from this reaction mixture as the first fraction by PLC.

[3]Rotaxane 11a. The tetracationic dumbbell-shaped compound **9a** (68 mg, 0.03 mmol) and BPP34C10 (161 mg, 0.3 mmol) were dissolved in dry MeCN (3 mL), and the reaction mixture was heated at 55 °C for 10 days. After cooling, MeCN was evaporated off at room temperature and Me_2CO (3 mL) was added. Crystalline BPP34C10 was filtered off and the red Me_2CO solution was purified by PLC [SiO_2, MeOH–CH_2Cl_2–$MeNO_2$ (7:2:1)] to give a red glassy solid (55 mg, 55%). **11a**: mp 150–153 °C (dec); FABMS 3030 (M - 2PF_6)⁺, 2885 (M - 3PF_6)⁺; ¹H NMR (CD_3COCD_3) δ 9.18 (4H, d, *J* = 6.5 Hz), 9.16 (4H, d, *J* = 6.5 Hz), 8.27 (4H, s), 8.24 (4H, d, *J* = 6.5 Hz), 8.00 (4H, s), 7.73 (4H, d, *J* = 8.5 Hz), 7.04–7.34 (34H, m), 6.84 (4H, d, *J* = 9 Hz), 6.23 (16H, s), 6.09 (4H, s), 6.04 (4H, s), 4.18–4.25 (4H, m), 4.09–4.16 (4H, m), 3.85–3.93 (8H, m), 3.76 (32H, bs), 3.72–3.76 (16H, m), 3.62–3.68 (16H, m), 1.29 (36H,s); ¹³C NMR (CD_3CN) δ 161.2, 157.7, 153.0, 149.6, 148.6, 147.4, 146.8, 146.6, 146.3, 145.4, 140.6, 135.8, 132.8, 132.6, 131.8, 131.6, 131.3, 128.6, 126.8, 126.2, 126.0, 125.5, 119.7, 118.3, 116.4, 115.7, 114.4, 71.4, 71.2, 70.7, 70.5, 70.3, 68.8, 65.5, 68.4, 65.0, 64.7, 64.4, 35.0, 31.6. Anal. ($C_{172}H_{202}N_4O_{26}P_4F_{24}$) C, H, N. The [2]rotaxane **10a** (17 mg, 20%) was also isolated from this reaction mixture as the second fraction by PLC.

[2]Rotaxane 10e and [3]Rotaxane 11e. Method A. BPP34C10 (117 mg, 0.22 mmol), the substituted benzylic chloride (307 mg, 0.43 mmol) freshly prepared from **6e**, and [BPYPYXY][PF_6]₂ (141 mg, 0.20 mmol) were dissolved in anhydrous DMF (8 mL), and the solution was placed in a Teflon ultra high pressure reaction vessel, which was subjected to a pressure of 12 kbar at 30 °C for 2 days. The reaction mixture was poured into H_2O (60 mL), and a saturated aqueous solution of NH_4PF_6 added. This solution was extracted with $MeNO_2$ (2 × 25 mL), and the organic layers were combined, washed with H_2O, and dried ($MgSO_4$). Removal of the solvent under reduced pressure gave a red oil, which afforded the [2]rotaxane **10e** (105 mg, 18%) and the [3]rotaxane **11e** (23 mg, 3%) pure after column chromatography [SiO_2, MeOH–CH_2Cl_2–CH_3NO_2–2M NH_4Cl (70:16:9:5), [3]rotaxane **11e** eluting from the column as the first product] **10e**: mp 260 °C (dec); FABMS 2606 (M - 2PF_6)⁺; ¹H NMR (CD_3COCD_3) δ 9.31 (4H, d, *J* = 6.5 Hz), 9.27 (4H, d, *J* = 6.5 Hz), 8.46 (4H, d, *J* = 6.5 Hz), 8.43 (4H, d, *J* = 6.5 Hz), 7.89 (4H, s), 7.66 (4H, d, *J* = 8.5 Hz), 7.23–7.29 (12H, m), 7.05–7.12 (20H, m), 6.82 (4H, d, *J* = 9 Hz), 6.23 (4H, s), 6.04 (12H, s), 4.18–4.22 (4H, m), 4.10–4.14 (4H, m), 3.85–3.92 (8H, m), 3.76 (32H, bs), 1.29 (54H, s); ¹³C NMR (CD_3COCD_3) δ 161.1, 157.7, 152.9, 149.4, 149.1, 148.0, 145.1, 140.3, 135.9, 132.7, 132.1, 131.4, 131.3, 127.3, 127.1, 125.9, 125.1, 124.9, 116.2, 115.6, 114.0, 71.3, 71.0, 70.7, 70.4, 70.2, 68.8, 68.3, 68.1, 65.1, 64.9, 63.8, 34.7, 31.5. Anal. ($C_{152}H_{178}N_4O_{16}P_4F_{24}$) C, H, N. **11e**: mp 218–223 °C (dec); ESMS 1571 (M - 2PF_6)²⁺; ¹H NMR (CD_3COCD_3) δ 9.18 (4H, d, *J* = 7 Hz), 9.16 (4H, d, *J* = 7 Hz), 8.26 (4H, d, *J* = 7 Hz), 8.23 (4H, d, *J* = 7 Hz), 8.00 (4H, s) 7.73 (4H, d, *J* = 8.5 Hz), 7.31 (12H, d, *J* = 8.5 Hz), 7.04–7.16 (20H, m), 6.83 (4H, d, *J* = 9 Hz), 6.22 (4H, s), 6.09 (16H, s), 6.04 (4H, s), 4.19–4.25 (4H, m), 4.09–4.17 (4H, m), 3.85 - 3.92 (8H, m), 3.76 (32H, s), 3.72–3.76 (16H, m), 3.62–3.68 (16H, m), 1.29 (54H, s); ¹³C NMR (CD_3CN) δ 161.2, 157.7, 153.0, 149.5, 146.8, 146.7, 146.3, 145.5, 140.8, 135.9, 132.7, 132.6, 131.8, 131.3, 126.0, 126.2, 125.4, 116.4, 115.7, 114.4, 71.4, 71.2, 70.7, 70.5,

70.3, 68.8, 68.5, 68.4, 64.7, 64.0, 35.0, 31.6, 30.3. Anal. ($C_{180}H_{218}N_4O_{26}P_4F_{24}$) C, H, N.

Method B. BPP34C10 (107 mg, 0.2 mmol), the substituted benzylic chloride (77 mg, 0.11 mmol) freshly prepared from **6e**, and [BPY-PYXY][PF$_6$]$_2$ (35 mg, 0.05 mmol) were dissolved in anhydrous DMF (2 mL). The solution was placed in a Teflon ultra high pressure reaction vessel and subjected to a pressure of 12 kbars at 30 °C for 2 days. The same workup and purification procedure gave **11e** (56 mg, 33%, first fraction) and **10e** (7 mg, 5%, second fraction).

Method C. The same reaction mixture, as employed in method A, was stirred at ambient pressure and room temperatute for 40 days. No rotaxane was isolated after the same workup procedure was applied as that described under method A.

***N,N′*-Bis(α-bromo-*p*-xylene)-4,4′-bipyridinium Bis(hexafluorophosphate) ([BBXYBIPY][PF$_6$]$_2$).** A solution of 4,4′-bipyridine (1.18 g, 7.6 mmol) in dry MeCN (200 mL) was added during 22 h to a refluxing solution of 1,4-bis(bromomethyl)benzene (20.0 g, 75.7 mmol) in dry MeCN (100 mL). Heating under reflux was maintained for another 2 h. After cooling down to room temperature, the suspension was filtered off, and the solid was washed with CH$_2$Cl$_2$ (200 mL) and then with H$_2$O (1.5 l). A saturated aqueous solution of NH$_4$PF$_6$ was added to the aqueous solution until no further precipitation was observed. The precipitate was filtered off and washed with H$_2$O (100 mL) to afford [BBXYBIPY][PF$_6$]$_2$ as a white crystalline solid (3.60 g, 58%): mp 260 °C (dec); MS (FAB) 669 (M - PF$_6$)$^+$, 524 (M - 2PF$_6$)$^+$; ^{1}H NMR (CD$_3$COCD$_3$) δ 9.53 (4H, d, *J* = 7 Hz), 8.83 (4H, d, *J* = 7 Hz), 7.67 (4H, d, *J* = 8 Hz), 7.60 (4H, d, *J* = 8 Hz), 6.18 (4H, s), 4.68 (4H, s); ^{13}C NMR (CD$_3$COCD$_3$) δ 151.5, 146.8, 141.1, 134.1, 131.0, 130.4, 128.5, 65.2, 33.1. Anal. ($C_{26}H_{24}Br_2F_{12}N_2P_2$) C, H, N.

***N,N′*-Bis[α-[4-(4-pyridyl)pyridinium]-*p*-xylylene]-4,4′-bipyridinium Tetrakis(hexafluorophospate) ([BPYPYXYBIPY][PF$_6$]$_4$).** A solution of [BBXYBIPY][PF$_6$]$_2$ (3.36 g, 4.1 mmol) and 4,4′-bipyridine (1.42 g, 9.1 mmol) in dry MeCN (300 mL) was heated under reflux for 6 h. After cooling down to room temperature, the reaction mixture was concentrated in vacuo to give a yellow solid, which was washed with CH$_2$Cl$_2$ (100 mL). Purification of the residue by column chromatography [SiO$_2$, MeOH−2 M NH$_4$Cl−MeNO$_2$ (5:4:1)] gave a solid which was dissolved in H$_2$O (500 mL). A saturated aqueous solution of NH$_4$PF$_6$ was added to this aqueous solution until no further precipitation was observed. The precipitate was filtered off and washed with H$_2$O (100 mL) to afford [BPYPYXYBIPY][PF$_6$]$_4$ as a white crystalline solid (2.05 g, 39%): mp 240 °C (dec); FABMS 1111 (M - PF$_6$)$^+$, 966 (M - 2PF$_6$)$^+$; ^{1}H NMR (CD$_3$COCD$_3$) δ 9.45 (4H, d, *J* = 7 Hz), 9.33 (4H, d, *J* = 7 Hz), 8.89 (4H, d, *J* = 6 Hz), 8.75 (4H, d, *J* = 7 Hz), 8.66 (4H, d, *J* = 7 Hz), 8.01 (4H, d, *J* = 6 Hz), 7.80 (8H, s), 6.22 (4H, s), 6.16 (4H, s); ^{13}C NMR (CD$_3$COCD$_3$) δ 155.4, 152.0, 151.6, 146.9, 146.4, 142.2, 136.1, 135.7, 131.3, 131.2, 128.6, 127.3, 122.8, 65.1, 64.5. Anal. ($C_{46}H_{40}F_{24}N_6P_4$) C, H, N.

***N,N′*-Bis[*N*-4-[2-[2-[4-ethylphenyl-bis(4-*tert*-butylphenyl)methoxy]-ethoxy]ethoxybenzyl-*N′*-*p*-xylylene]-4,4′-bipyridinium Hexakis(hexafluorophospate) (12c).** The tetrakis(hexafluorophosphate) derivative [BPYPYXYBIPY][PF$_6$]$_4$ (770 mg, 0.61 mmol) and the substituted benzyl chloride (420 mg, 0.61 mmol) freshly prepared from **6c** were dissolved in anhydrous DMF (9 mL) and placed in a Teflon ultra high pressure reaction vessel. The reaction mixture was subjected to a pressure of 12 kbar at 50 °C for 40 h. The precipitation from the resulting heterogenous reaction mixture was completed by adding Et$_2$O (30 mL). The solid was filtered off and then dissolved in a mixture of Me$_2$CO−H$_2$O. A saturated aqueous solution of NH$_4$PF$_6$ was added, and the Me$_2$CO was evaporated off to afford a white solid. The filtered solid was dried under vacuum and then combined with the DMF solution, obtained from the initial DMF−Et$_2$O filtrate by evaporation of Et$_2$O. Another portion of the chloride (420 mg, 0.61 mmol, freshly prepared from **6c**) was added, and the homogenous solution was subjected to a pressure of 12 kbar at 50 °C for another 40 h. The same workup procedure as employed above was repeated, and another portion of the chloride was added (420 mg, 0.61 mmol). The reaction mixture was treated under the same conditions (12 kbar, 50 °C, 40 h). The solvent was removed under vacuum to give a yellowish solid. After counterion exchange (Me$_2$CO−H$_2$O, saturated aqueous solution of NH$_4$PF$_6$), column chromatography (SiO$_2$, 0.08 M NH$_4$PF$_6$ in Me$_2$CO) afforded pure **12c** (742 mg, 42%): mp

260 °C (dec); FABMS 2709 (M - PF$_6$)$^+$, 2564 (M - 2PF$_6$)$^+$, 2419 (M − 3PF$_6$)$^+$; ^{1}H NMR (CD$_3$COCD$_3$), δ 9.46 (12H, d, *J* = 7 Hz), 8.72−8.82 (12H, m), 7.79 (8H, s), 7.63 (4H, d, *J* = 9Hz), 7.31 (8H, d, *J* = 9 Hz), 7.04−7.15 (24H, m), 6.95 (4H, d, *J* = 9 Hz), 6.22 (8H, s), 6.10 (4H, s), 4.20 (4H, m), 4.14 (4H, m), 3.85−3.92 (8H, m), 2.61 (4H, q, *J* = 8Hz), 1.29 (36H, s), 1.20 (6H, t, *J* = 8 Hz); ^{13}C NMR (CD$_3$COCD$_3$) δ 161.2, 157.8, 151.6, 151.4, 151.2, 149.2, 146.9, 146.5, 145.8, 145.2, 142.4, 140.4, 135.7, 132.8, 132.1, 131.7, 131.4, 131.3, 128.6, 128.4, 127.6, 125.8, 125.0, 116.3, 114.1, 70.5, 70.3, 68.6, 68.2, 65.4, 65.0, 64.0, 34.8, 31.6, 28.7, 15.7. Anal. ($C_{138}H_{146}F_{36}N_6O_6P_6$) C, H, N.

[2]Rotaxane 13c, [3]Rotaxane 14c, and [4]Rotaxane 15c. Method A. The hexacationic dumbbell-shaped compound **12c** (40 mg, 0.015 mmol) and BPP34C10 (170 mg, 0.32 mmol) were dissolved in MeCN (4 mL). The reaction mixture was heated at 50 °C for 10 days. Removal of MeCN afforded a red solid, which was subjected to column chromatography [SiO$_2$, MeOH−2 M NH$_4$Cl−MeNO$_2$, (7:2:1)] to afford pure **13c** (2 mg, 1%): mp 220 °C (dec); ESMS 1550 (M - 2PF$_6$)$^{2+}$, 985 (M - 3PF$_6$)$^{3+}$, 702 (M - 4PF$_6$)$^{4+}$; ^{1}H NMR (CD$_3$COCD$_3$) δ 9.31−9.40 (12H, m), 8.50−8.64 (12H, m), 7.86 (8H, s), 7.66 (4H, d, *J* = 9 Hz), 7.31 (8H, d, *J* = 9 Hz), 7.06−7.15 (24H, m), 6.84 (4H, d, *J* = 9 Hz), 6.21 (8H, s), 6.07 (12H, s), 4.17−4.23 (4H, m), 4.10−4.16 (4H, m), 3.85−3.93 (8H, m), 3.71−3.80 (24H, m), 3.63−3.69 (24H, m), 2.61 (4H, q, *J* = 8 Hz), 1.29 (36H, s), 1.20 (6H, t, *J* = 8 Hz); ^{13}C NMR (CD$_3$COCD$_3$) δ 162.7, 161.2, 157.8, 153.0, 150.2, 149.8, 149.2, 146.8, 146.5, 145.6, 145.2, 142.4, 140.4, 135.9, 132.8, 132.2, 131.7, 131.4, 127.8, 127.7, 127.6, 127.5, 126.0, 125.0, 116.3, 115.7, 114.1, 71.4, 71.1, 70.8, 70.5, 70.3, 68.6, 68.4, 68.2, 65.2, 64.9, 63.9, 34.8, 31.6, 28.8, 15.8. Anal. ($C_{166}H_{186}F_{36}N_6O_{16}P_6$) C, H, N. **14c** (7 mg, 12%): mp 197 °C (dec); ESMS 1818 (M - 2PF$_6$)$^{2+}$, 1164 (M - 3PF$_6$)$^{3+}$, 837 (M - 4PF$_6$)$^{4+}$, ^{1}H NMR (CD$_3$COCD$_3$) δ 9.19−9.32 (12H, m), 8.38−8.49 (8H, m), 8.33 (4H, d, *J* = 7 Hz), 7.93 (8H, s), 7.70 (4H, d, *J* = 9 Hz), 7.31 (8H, d, *J* = 9 Hz), 7.06−7.15 (24H, m), 6.84 (4H, d, *J* = 9 Hz), 6.21 (8H, s), 6.08 (16H, s), 6.06 (4 H, s), 4.18−4.24 (4H, m), 4.10−4.16 (4H, m), 3.85−3.94 (8H, m), 3.71−3.80 (48H, m), 3.63−3.69 (16H, m), 2.60 (4H, q, *J* = 8 Hz), 1.29 (36H, s), 1.20 (6H, t, *J* = 8 Hz); ^{13}C NMR (CD$_3$COCD$_3$) δ 161.2, 157.8, 153.0, 149.8, 149.2, 146.8, 146.4, 145.6, 145.2, 142.4, 140.3, 136.0, 135.9, 132.8, 132.3, 131.7, 131.6, 131.5, 131.4, 127.6, 127.1, 126.9, 126.8, 126.1, 125.0, 116.3, 115.7, 114.1, 71.3, 71.1, 70.8, 70.5, 70.3, 68.6, 68.4, 68.2, 65.1, 64.8, 64.7, 63.9, 34.8, 31.6, 28.8, 15.8. Anal. ($C_{194}H_{226}F_{36}N_6O_{26}P_6$) C, H, N. **15c** (13 mg, 19%): mp 148 °C (dec); ESMS 2087 (M - 2PF$_6$)$^{2+}$, 1343 (M - 3PF$_6$)$^{3+}$; ^{1}H NMR (CD$_3$COCD$_3$) δ 9.10−9.20 (12H, m), 8.28−8.19 (12H, m), 7.98 (8H, s), 7.73 (4H, d, *J* = 9 Hz), 7.26−7.34 (8H, m), 7.05−7.15 (24H, m), 6.63 (4H, d, *J* = 9 Hz), 6.21 (8H, s), 6.08 (16H, s), 6.06 (8H, s), 6.03 (4H, s), 4.19−4.25 (4H, m), 4.10−4.16 (4H, m), 3.85−3.93 (8H, m), 3.70−3.79 (72H, m), 3.61−3.69 (24H, m), 2.61 (4H, q, *J* = 8 Hz), 1.29 (36H, s), 1.20 (6H, t, *J* = 8 Hz); ^{13}C NMR (CD$_3$COCD$_3$) δ 161.1, 157.8, 152.9, 152.8, 149.1, 147.3, 147.0, 146.8, 146.7, 146.3, 145.5, 145.2, 142.3, 140.3, 136.1, 132.8, 134.2, 131.6, 131.3, 128.8, 127.6, 126.3, 126.2, 126.1, 126.0, 125.0, 116.1, 115.6, 115.0, 114.1, 114.0, 71.4, 71.3, 71.0, 70.7, 70.5, 70.4, 70.3, 68.8, 68.6, 68.3, 68.1, 64.8, 64.6, 63.9, 34.8, 31.6, 28.8, 15.8. Anal. ($C_{222}H_{266}F_{36}N_6O_{36}P_6$) C, H, N. The [4]rotaxane **15c** was obtained as the first fraction, followed by the [3]rotaxane **14c** and the [2]rotaxane **13c**, respectively.

Method B. The hexacationic dumbbell-shaped compound **12c** (250 mg, 0.088 mmol) and BPP34C10 (94 mg, 0.175 mmol) were dissolved in MeCN (4 mL) and heated at 50 °C for 10 days. The removal of MeCN afforded a red solid, which was subjected to column chromatography [SiO$_2$, MeOH−2 M NH$_4$Cl−MeNO$_2$, (7:2:1)] to afford pure **15c** (15 mg, 4%), **14c** (33 mg, 10%), and **13c** (56 mg,19%), respectively.

[3]Rotaxane 14e and [4]Rotaxane 15e. BPP34C10 (234 mg, 0.44 mmol), the substituted benzylic chloride (307 mg, 0.43 mmol) freshly prepared from **6e**, and [BPYPYXYBIPY][PF$_6$]$_4$ (251 mg, 0.2 mmol) were dissolved in anhydrous DMF (10 mL). The reaction mixture was placed in a Teflon ultra high pressure reaction vessel and subjected to a pressure of 12 kbar at 30 °C for 6 days. The same workup procedure as that described for **10e** and **11e** gave a red solid, which afforded the pure [3]rotaxane **14e** (9 mg, 1%) and the pure [4]rotaxane **15e** (26 mg, 3%) after PLC (SiO$_2$, 0.5% solution of NH$_4$PF$_6$ in Me$_2$CO). **14e**: mp 225−230 °C (dec); ESMS 1846 (M - 2PF$_6$);$^{2+}$ ^{1}H NMR (CD$_3$COCD$_3$)

Self-Assembly of [n]Rotaxanes

J. Am. Chem. Soc., Vol. 118, No. 21, 1996 4951

δ 9.29 (4H, d, $J = 7$ Hz), 9.27 (4H, d, $J = 7$ Hz), 9.23 (4H, d, $J = 7$ Hz), 8.45 (4H, d, $J = 7$ Hz), 8.42 (4H, d, $J = 7$ Hz), 8.34 (4H, d, $J = 7$ Hz), 7.93 (8H, s), 7.70 (4H, d, $J = 9$ Hz), 7.32 (12H, d, $J = 8.5$ Hz), 7.06−7.16 (20H, m), 6.85 (4H, d, $J = 9$ Hz), 6.22 (8H, s), 6.09 (16H, s), 6.06 (4H, s) 4.18−4.25 (4H, m), 4.11−4.17 (4H, m), 3.86−3.93 (8H, m), 3.75 (48H, br s), 3.63−3.69 (16H, m), 1.30 (54H, s). **15e**: mp 175−179 °C (dec); ESMS 2115 (M − 2PF$_6$)$^{2+}$, 1362 (M − 3PF$_6$)$^{3+}$; ^{1}H NMR (CD$_3$COCD$_3$) δ 9.17 (4H, d, $J = 7$ Hz), 9.16 (4H, d, $J = 7$ Hz), 9.14 (4H, d, $J = 7$ Hz), 8.25 (4H, d, $J = 7$ Hz), 8.22 (4H, d, $J = 7$ Hz), 8.21 (4H, d, $J = 7$ Hz), 7.98 (8H, s), 7.73 (4H, d, $J = 9$ Hz), 7.31 (12H, d, $J = 8.5$ Hz), 7.06−7.16 (20H, m), 6.83 (4H, d, $J = 9$ Hz), 6.22 (8H, s), 6.09 (16H, s), 6.07 (8H, s), 6.04 (4H, s), 4.19−4.25 (4H, m), 4.10−4.16 (4H, m), 3.86−3.93 (8H, m) 3.75 (48H, s), 3.73 (24H, s), 3.61−3.69 (24H, m), 1.30 (54H, s); ^{13}C NMR (CD$_3$CN) δ 161.2, 157.7, 153.0, 152.9, 149.5, 146.8, 146.6, 146.3, 145.5, 140.7, 135.8, 132.7, 132.6, 131.8, 131.2, 126.1, 126.0, 125.5, 116.4, 115.7, 114.3, 71.4, 71.2, 70.7, 70.5, 70.3, 68.5, 68.4, 64.7, 64.0, 35.0, 31.6. Anal. (C$_{226}$H$_{274}$N$_6$O$_{36}$P$_6$F$_{36}$) C, H, N. The [4]rotaxane **15e** was obtained as the first compound to be eluted from the column, followed by the [3]rotaxane **14e**.

Association Constants. The stability constants (K_a) for the 1:1 complexes between BPP34C10 and the bipyridinium-based guests [BHBIPY][PF$_6$]$_2$, [BHEBIPY][PF$_6$]$_2$, and [BHEEBIPY][PF$_6$]$_2$ were evaluated by probing the charge-transfer band of the complexes by UV−vis spectroscopy and employing the titration methodology.[17] Progressive addition of the guests to a Me$_2$CO solution of BPP34C10 at fixed concentration (*ca.* 10^{-3} M) results in the increase of the intensity of the charge-transfer band of the complexes. Treatment of the collected data with a nonlinear curve-fitting program operated on a Apple Macintosh microcomputer afforded the K_a values.

Rate Constants. The formation of the [2]rotaxanes **8a−c** was monitored by following the charge-transfer band by UV−vis spectroscopy. BPP34C10 and each of the dumbbell-shaped compounds **7a−d** were mixed together in dry MeCN in the relative molar proportions of 4:1. The resulting solutions were placed in a quartz cuvette, and the change of the UV−vis spectrum was followed in the range between 220 and 600 nm over a period of 60 h by means of a computer-controlled Perkin-Elmer Lambda 2 spectrophotometer fitted with a thermostatic temperature controller (control $\pm$ 0.2 °C). The data aquisition was performed on a fresh sample at seven different temperatures in the range between 298 and 333 K for each of the bipyridinium salts **7a−d**. Treatment of the collected data, with a nonlinear curve-fitting program operated on a Apple Macintosh microcomputer, afforded the rate constants values.

X-ray Crystallography. Single crystals of the 1:1 complexes [BPP34C10-BHBIPY][PF$_6$]$_2$, [BPP34C10-BHEBIPY][PF$_6$]$_2$, and [BPP34C10-BHEEBIPY][PF$_6$]$_2$ suitable for X-ray crystallographic analysis were grown by vapor diffusion of *i*-Pr$_2$O into equimolar solutions of the components in Me$_2$CO. X-ray crystallography data were measured[2d] on a Nicolet R3m diffractometer with graphite monochromated Cu-K$_\alpha$ radiation with ω scans. Atomic coordinates, bond lengths and angles, thermal parameters can be obtained from the Cambridge Crystallographic Data Centre, 12 Union Road, GB-Cambridge CB2 1EZ (UK).

Absorption and Luminescence Measurements. Room temperature experiments were usually carried out in MeCN solutions. Electronic absorption spectra were recorded with a Perkin-Elmer Lamba 6 spectrophotometer. Emission spectra and phosphorescence lifetimes were obtained with a Perkin-Elmer LS5O spectrofluorimeter. Emission spectra in butyronitrile rigid matrix at 77 K were recorded using quartz tubes immersed in a quartz Dewar filled with liquid nitrogen. Fluorescence quantum yields were determined using naphthalene in degassed cyclohexane as a standard ($\Phi = 0.23$).[29] Nanosecond and picosecond lifetime measurements were performed with a previously described Edinburgh single-photon counting equipment and a picosecond spectrometer based on a Nd:YAG (PY62−10 Continuum) laser and a Hamamatsu C1587 streak camera.[30] Experimental errors: absorption maxima, ± 2 nm; emission maxima, ± 2 nm; excited state lifetimes, $\pm 10\%$; fluorescence quantum yields, $\pm 20\%$.

Electrochemical Measurements. Electrochemical experiments were carried out in Ar-purged MeCN solution with a Princeton Applied Research 273 multipurpose instrument interfaced to a personal computer, using cyclic voltammetry (CV) and differential pulse voltammetry (DPV) techniques. The working electrode was a glassy carbon electrode (0.08 cm^2, Amel); its surface was routinely polished with a 0.05 μm alumina-water slurry on a felt surface immediately prior to use. The counter electrode was a Pt wire, and the reference electrode was a satured calomel electrode (SCE) separated with a fine glass frit. The concentration of the examined compounds was 5.0×10^{-4} M; 0.05 M [Et$_4$N][PF$_6$] was added as supporting electrolyte. Cyclic voltammograms were obtained at sweep rates of 20, 50, 200, 500, and 1000 mV s^{-1}; DPV experiments were performed with a scan rate of 20 mV s^{-1}, a pulse height of 75 mV, and a duration of 40 ms. For reversible processes, the halfwave potential values are reported; the same values are obtained from the DPV peaks and from an average of the cathodic and anodic cyclic voltammetric peaks. For irreversible processes, the reported potential values are those evaluated from the DPV peaks. Both CV and DPV techniques have been used to measure the number of the exchanged electrons in each redox process; since the results obtained for irreversible processes can be unreliable, no quantitative conclusions have been drawn on the number of electrons exchanged in the oxidation processes. To establish the reversibility of a process, we used the criteria of (i) separation between cathodic and anodic peaks, (ii) close to unity ratio of the intensities of the cathodic and anodic currents, and (iii) constancy of the peak potential on changing sweep rate in the cyclic voltammograms. The experimental error on the potential values was estimated to be ± 20 mV.

Supporting Information Available: Derivation of eqs 1−3 for the determination of the first order rate constants k_1 and k_2 associated with the process illustrated in Table 5 (2 pages). Ordering information is given on any current masthead page.

JA954334D

(29) Berlman, *Handbook of Fluorescence Spectra of Aromtic Compounds*, Academic Press: London, 1965.

(30) Armaroli, N.; Balzani, V.; Barigelletti, F.; De Cola, L.; Flamigni, L.; Sauvage, J. P.; Hemmert, C. *J. Am. Chem. Soc.* **1994**, *116*, 5211−5217.